Rotating disk atomization of Gd and Gd-Y for hydrogen liquefaction via magnetocaloric cooling

by

Tyler J Slinger

A thesis submitted to the graduate faculty

in partial fulfillment of the requirements for the degree of

MASTER OF SCIENCE

Major: Materials Science

Program of Study Committee:
Iver E. Anderson, Major Professor
L. Scott Chumbley
Frank Peters

Iowa State University

Ames, Iowa

2016

TABLE OF CONTENTS

LIST OF FIGURES

LIST OF TABLES

ACKNOWLEDGMENTS

I would like to thank my advisor Iver Anderson for inspiring not only this work, but myself. I would like to extend my gratitude to Dave Byrd, Ross Anderson and Trevor Riedemann for their technical expertise in making the atomization experiments work and Micheal Ambrose, Dustin Hoffman, and Alex Benson for all their help with this project. I wish to also thank Brandt Jensen for his magnetic property measurements and his insight into these alloys. Finally, I would like to acknowledge the financial support from the U.S. Department of Energy, Office of Energy Efficiency and Renewable Energy, Fuel Cell Technologies Office at the Ames Laboratory under contract number DE-AC02-07CH11358.

ABSTRACT

In order to enable liquid hydrogen fuel cell technologies for vehicles the cost of hydrogen liquefaction should be lowered. The current method of hydrogen liquefaction is the Claude cycle that has a figure of merit (FOM) of 0.3-0.35. New magnetocaloric hydrogen liquefaction devices have been proposed with a FOM>0.5, which is a significant improvement. A significant hurdle to realizing these devices is the synthesis of spherical rare earth based alloy powders of 200μm in diameter. In this study a centrifugal atomization method that used a rotating disk with a rotating oil quench bath was developed to make gadolinium and gadolinium-yttrium spheres. The composition of the spherical powders included pure Gd and $Gd_{0.91}Y_{0.09}$. The effect of atomization parameters, such as superheat, melt properties, disk shape, disk speed, and melt system materials and design, were investigated on the size distribution and morphology of the resulting spheres. The carbon, nitrogen, and oxygen impurity levels also were analyzed and compared with the magnetic performance of the alloys. The magnetic properties of the charge material as well as the resulting powders were measured using a vibrating sample magnetometer. The saturation magnetization and Curie temperature were the target properties for the resulting spheres. These values were compared with measurements taken on the charge material in order to investigate the effect of atomization processing on the alloys.

CHAPTER 1

INTRODUCTION

Purpose of Study

One of the barriers to fuel cell electric vehicle technology is the delivery of hydrogen to fueling stations. Liquid hydrogen is the ideal form of delivery due to its higher volumetric and gravimetric energy density [1]. Current commercial hydrogen liquefiers use a liquid nitrogen pre-cooled Claude cycle [7]. This method of liquefaction has a figure of merit (FOM) between .3-.35. This means the ratio of the ideal work input per unit mass of liquefied gas to the real work input is .3-.35. In order to make this technology more viable the cost of liquid hydrogen must be decreased by increasing the efficiency of the liquefaction process [7].

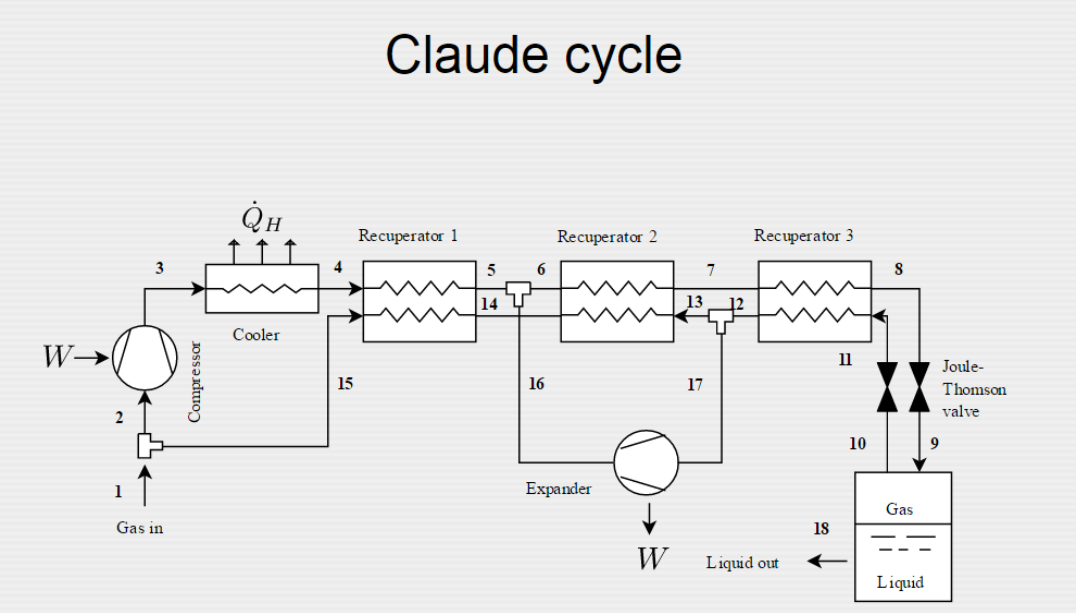

Figure 1: Claude cycle schematic [29]

Magnetocaloric refrigeration has a greater thermodynamic efficiency than the Claude cycle [30]. Theoretically, an efficient refrigerator could achieve liquefaction with a FOM >0.5. There are several barriers to constructing this type of refrigerator and the focus of this work is the processing of rare-earth magnetocaloric materials.

MagnetoCaloric Effect

The Magnetocaloric effect relies on the decrease in magnetic entropy that occurs when a magnetic field is applied to a ferromagnetic material. This causes the material's temperature to increase. Heat can be rejected and when the magnetic field is removed, the material cools. This effect is most intense when the material is at its Curie temperature (see Figure 2) [3].

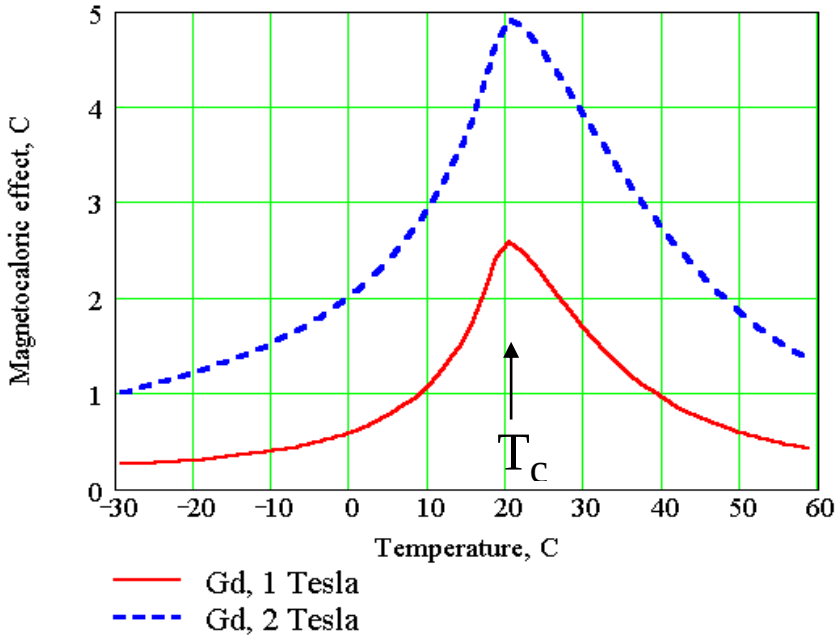

Figure 2: Magnetocaloric effect in Gadolinium [2]

By using a series of alloys with decreasing Curie temperature efficiency can be increased by making the operating temperature that the alloy is used near to its Curie temperature. The cooling of the magnetocaloric material upon removal of the magnetic field can then be exploited to cool a load, in this case hydrogen.

Production Techniques

In order to maximize the efficiency of the liquefaction process heat needs to be transferred efficiently between the magnetocaloric material, the heat sink, and the hydrogen gas. This requires the Lanthanide materials to be processed into spheres of 200 micron diameter for efficient refrigeration [6]. Smaller diameter powders have greater surface area, but restrict heat exchanger fluid flow through the powder bed. Larger powders have lower surface area and lower the heat exchange between the powder bed and heat exchange fluid [6]. Packing density which comes from powder morphology is also important and determines how much material can be influenced by the applied magnetic field. The reactivity of lanthanides as well as inherent limitations of some processing techniques restricts production techniques [4]. Techniques such as spark erosion and mechanical attrition have drawbacks of forming thick oxide layers and aspherical particles. Gas atomization produces spheres <100µm well but tend to have prominent internal porosity in larger powders [5]. This leaves the plasma rotating electrode process (PREP) and centrifugal atomization processes as the most viable methods for this application. We selected the

centrifugal atomization process due to its ability to create coarse (200μm), fully dense, spherical powders without heavy contamination of the powders.

Centrifugal Atomization

Centrifugal atomization is the disintegration of molten material by the centrifugal force generated by a rotating disk, cup, wheel, or ingot. Several methods of centrifugal atomization techniques can be found in Powder Metallurgy Science[8], or several reviews by Lawley [9,10].

For this study, centrifugal atomization via a rotating disk was used to create molten droplets. In this two-step process the liquid is first melted in a crucible, in this case above the disk, then poured onto a rotating disk.

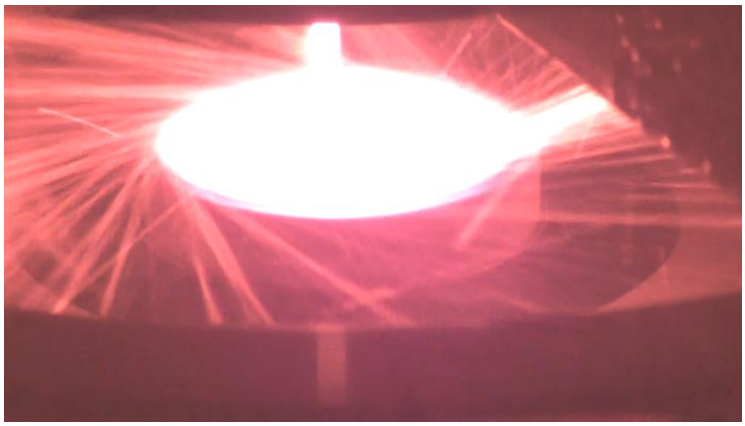

Figure 3: Rotating Disk Atomization

Molten metal wets the disk and flows towards the periphery of the disk where it forms a liquid torus. Instabilities caused by the disk's rotation create small ligaments at the edge of the disk which then fling off the disk in the form of droplets. At higher liquid supply rates, ligaments may not form and film disintegration mode will occur. At low liquid supply

rates droplets may form directly at the edge of the disk or be produced before the edge of the disk due to incomplete wetting of the disk [12].

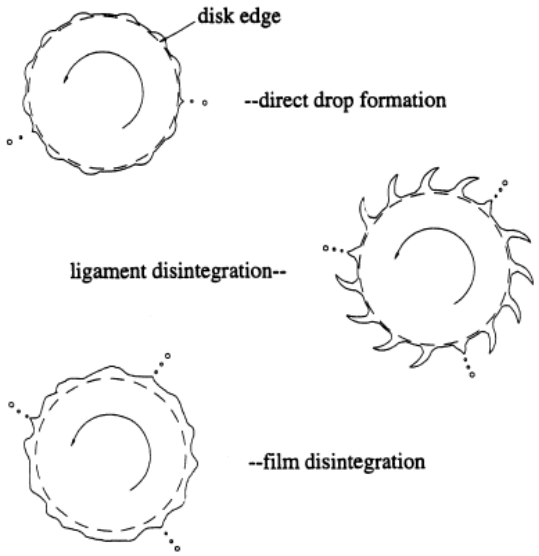

Figure 4: Atomization modes from rotating disk atomization [11]

Attempts have been made to derive conditions for these transitions (Fig. 4) as empirically it has been found that operating in the direct droplet mode produces the lowest standard deviation of droplet sizes[11,12].

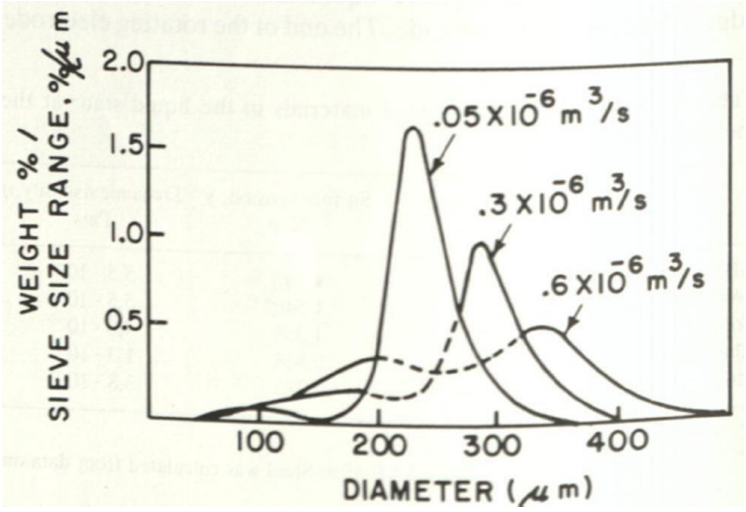

Figure 5: Size distribution depending on melt flow rate and atomization mechanism [11]

An empirical formula developed by Champagne and Angers for rotating electrode atomization predicts the mass mean particle diameter of centrifugally atomized particles [13]:

$$d_{50} = 3.65\left(1/\omega\right)\left(\gamma/\rho\right)^{0.46}\left(1/D^{0.58}\right)Q^{0.06}$$

Eqn. 1

Where:
d_{50} =mean particle diameter by mass (m)
ω = angular speed(radians/sec)
γ =surface energy(N/m)
ρ = liquid density(kg/m^3)
Q = liquid flow rate (m^3/s)

This formula has also been a good predictor of other pure metal rotating disk atomizations [14,15]. The liquid flow rate in this case goes from highest at the runs beginning due to metal head pressure being the greatest at the beginning and lowering as the metal drains from the crucible. To compensate for this the average value is used in Eqn. 1.

After the melt has been flung from the disk in droplet form there are several ways that solidification can occur. The simplest is the case of no quenchant where the droplet solidifies in flight. Gas jets have also been used to aid in cooling as well as various forms of quenchant [16,17]. Due to the limited size of the inert chamber used in this study a rotating oil quench bath is used to solidify powders before splatting against the chamber wall.

CHAPTER 2

EQUIPMENT AND PROCEDURE

Inert Chamber

The atomization chamber is evacuated with a roughing pump and backfilled with high purity argon three times prior to all atomizations. After the third backfill of the chamber, argon is bled into the system and allowed to escape simultaneously. The inside of the chamber is allowed to reach a steady state of 1psi overpressure. This ensures that the atmosphere in the chamber is as free from as many contaminants as possible.

Melt System

Due to the reactivity of lanthanides a tantalum crucible and stopper rod were used for most of the atomization trials (see Fig. 6). One trial was conducted using a yttria-lined, yttria stabilized zirconia (YSZ) ceramic crucible with a tantalum stopper rod as a test for this type of melt system. In all cases the hollow stopper rod has a thermocouple fed through to the tip to monitor the temperature of the melt. The stopper rod starts in the down position plugging the orifice at the bottom of the crucible. An induction coil is used to heat the tantalum crucible and charge and in the case of the ceramic crucible, the induction coil heats a tantalum susceptor that radiates heat through the ceramic and into the charge. Once the charge is molten and the desired superheat is achieved the stopper rod is lifted pneumatically and the crucible drains. The crucibles in this study had a 2.6mm opening except for the

ceramic crucible which had a 3mm opening. The opening size can help control the liquid supply rate onto the disk. In past iterations of the atomizer a pressurized crucible was used to control liquid supply rate during the atomization of Calcium, however this method is impractical for larger batches of higher melting metals due to the larger orifice needed for higher melt flow rates [27].

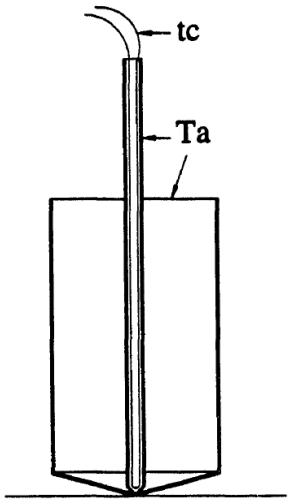

Figure 6: Schematic of crucible and stopper rod with a thermocouple feed through

Atomization Disk and Drive Motor

The atomization disk in this study was a 0.015in thick Tantalum disk in all cases. The geometry and disk diameter were varied from run to run in order to affect the powder distribution (see Eqn 1), and to ensure that liquid droplets are consistently coming from the edge of the disk. This is important for the mean particle size as well as the standard deviation of the powder size distribution [13]. Cupped, or disks with raised edges have been shown to provide a tighter, finer powder size distribution [18].

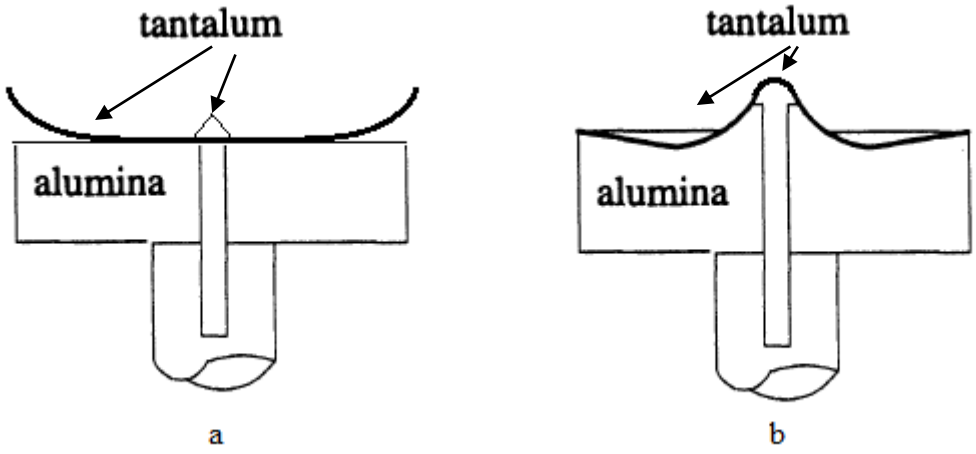

Figure 7: Disk designs used

No coatings were used in this work due to tantalum being one of the few compatible metals with lanthanides, however improved wetting can be achieved in some cases with the use of coatings [19]. This study also uses an alumina backing to the thin tantalum disk. This allows the disk to get "hot" after a short time as it is insulated from underneath. This helps prevent a frozen metal layer, or skull from being formed on the disk which causes inconsistent breakup of the powders [17].

The disk is spun by a DC router motor mounted outside of the atomization chamber. There is a magnetic coupler that allows the motor shaft to spin the disk inside the inert chamber. After the charge is molten the disk is spun prior to the stopper rod being lifted allowing the disk to reach its set speed before the melt impinges on it.

Quench Bath

A rotating quench bath is used due to the limited size of the inert chamber. Since spherical shapes are desired, the droplets must be quenched before they hit a chamber wall. The rotation of the quench bath allows the oil to cover the quench bath wall (Figure 8) to prevent molten droplets from splatting. After the inert chamber is argon purged the quench bath rotation is started and spun to around 210 RPM.

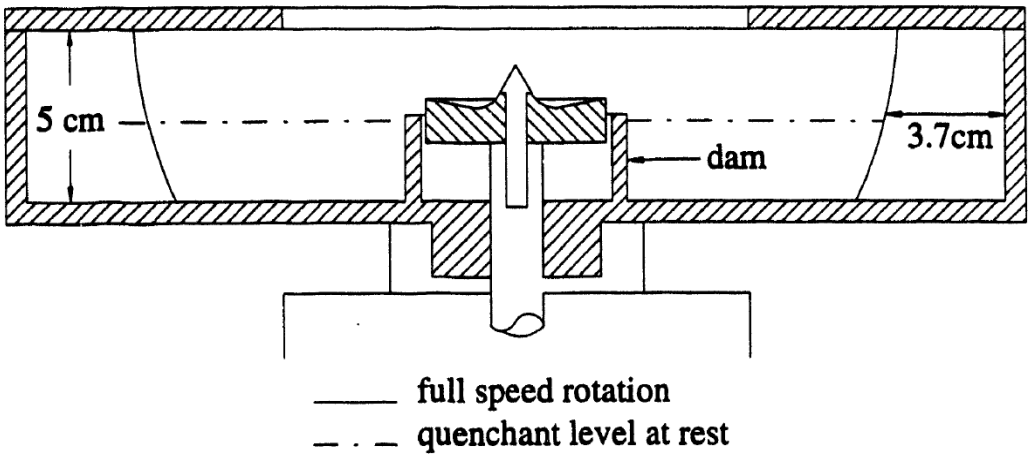

Figure 8: Rotating quench bath

The quench bath is filled with 1.5L of KJLC 704 Silicone Pump fluid. Silicone oils tend to be more stable than hydrocarbon oils and this oil has a relatively low viscosity of 37dynes/cm [32]. The amount of heat added to the oil from the atomization runs was calculated based on the mass of gadolinium melted. Using the mass of the oil and its specific heat the temperature rise of the oil was determined to be at most 110°C which is well below the flash point of 220°C. This type of oil prevents oil degradation from the molten metal contacting it. The low viscosity allows less secondary atomization of the powders which is the process of droplets deforming or further breaking up on contact with the oil or walls.

Further, the oil has an effect on the surface chemistry of the powders. The oil has shown to be passivating in the past for this type of material [14].

Charge Material

The cleanliness of charge material is important to the success of these atomization runs. In the first atomization attempt reduced purity Gadolinium was used that had been processed in tungsten. The run would not pour despite the stopper rod being lifted and the coil eventually had to be turned off (Fig 9).

Figure 9: Cross section crucible at orifice showing area of tungsten agglomeration (Fig. 10)

Scanning electron microscope images with EDS scans showed clumps of tungsten particles that agglomerated gadolinium oxides to the bottom of the crucible. These solid agglomerations appear to block the melt flow at the orifice (Fig. 10).

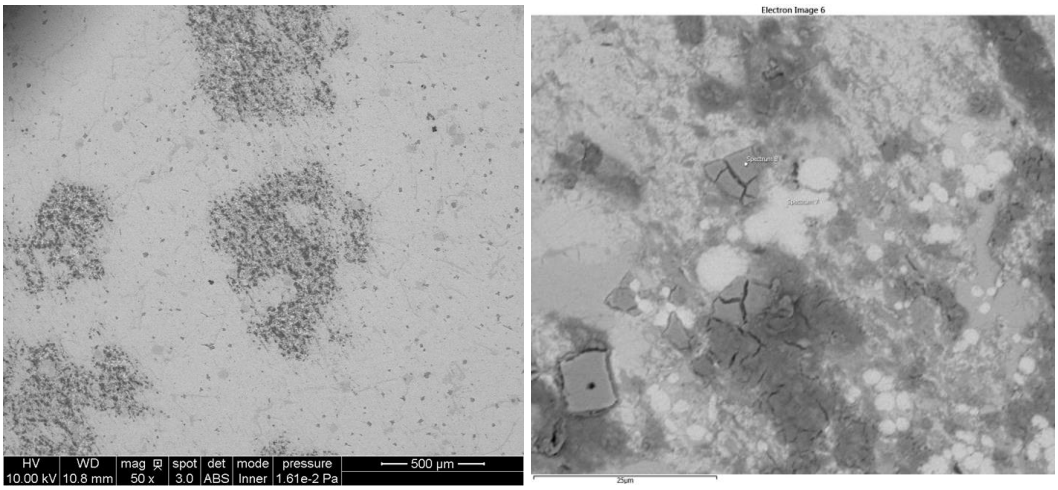

Figure 10: SEM images showing oxides(dark) and tungsten particles(light) near the crucible orifice

Despite less than 1 at% tungsten in the charge material the orifice was blocked. After switching charge materials to tantalum processed material the problem no longer occurred.

Procedure

Once the melt has reached the desired superheat and is held for ~30s the stopper rod is lifted. Video of the run is recorded, but the chamber fills with smoke/vapor from the quench oil within a few seconds of the run beginning. The crucible empties within 30-75s depending on the charge mass and the disk is stopped. The chamber is sealed, evacuated, and backfilled with argon to allow cooling.

After the system has cooled overnight, the inert chamber is opened and the quench bath is removed. Used oil is siphoned off and disposed of. The powder is then extracted into a container for washing. First, acetone is added and the container is agitated. The acetone is siphoned off with a pipette and this process is repeated 4-6 times until the acetone becomes clear colored indicating most of the oil is removed from powder surfaces. This is followed by

two ethanol washes in the same manner and then two hexane washes to ensure the surfaces of the powder are clean. The material is sieved to a size of below 1mm to ensure that shed skulls, large flakes, and alumina pieces are removed. Then the powder is sieved in a screen stack of 250, 150, and 45µm. Samples are taken for microtac, LECO analysis, Magnetic testing, and SEM imaging.

Table 1: Atomization Parameters

Run I.D	Crucible	S. Rod	Disk Diam	RPM	Superheat °C	C. Mass (g)	C. Material
RDA-1	Cer	Ta	2 in	8000	127	489.4	Gd, PREP
RDA-2	Ta	Ta	1.7 in	8000	117	1002.9	Gd, HEFA
RDA-3	Ta	Ta	1.7 in	8000	92	1258.9	Gd, HEFA
RDA-4	Ta	Ta	1.7 in	8000	95	1343.7	$Gd_{.91}Y_{.09}$
RDA-5	Ta	Ta	2 in	19290	91	1524.6	$Gd_{.91}Y_{0.9}$

CHAPTER 3

POWDER MORPHOLOGY

Gadolinium

Powder morphology effects how efficient the refrigeration process is in two ways. One is the packing density of the powder in the bed. This controls the mass of powder that is exposed to the high magnetic field. The more powder exposed the more cooling power a given volume of powder bed has. The second effect is how the helium used as heat exchanger fluid can flow through the powder bed. With flaky powders the flow is impeded which causes inefficient heat exchange. Therefore, spherical powders are desired for this process [20].

Images of powder particles from the first gadolinium run can be seen below (Fig. 11). There are very few spheres in this size range of powder which is the desired size range for the magnetocaloric material. This shape of material would not pack into the ideal density due to its shape and would also limit gas flow through a packed bed [20].

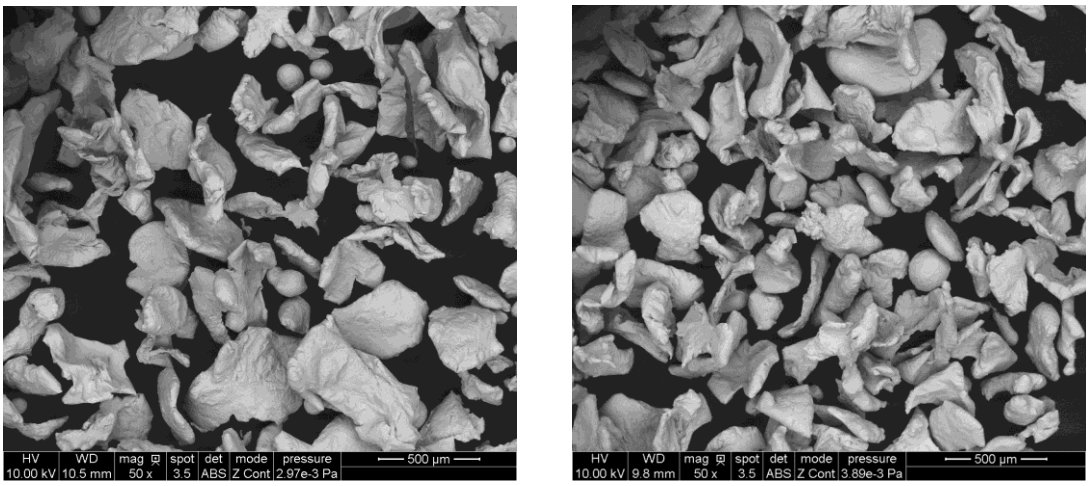

Figure 11: RDA-1 gadolinium powder image (150-250µm) sieve

In order to determine the cause of this morphology the spheroidization time for the molten droplets was calculated. The spheroidization time for these particles can be calculated by the following equation assuming the droplets formed as a cylinder with a 10:1 dimensional ratio [21]:

$$t_s = \frac{3\pi^2 \mu (R^4 - r^4)}{4 V_p \sigma} \qquad \textbf{Eqn. 2}$$

Where:

t_s=spheroidiztion time

μ=liquid viscosity

V_p=droplet volume

σ=surface tension

Applying values for gadolinium [22] gives a spheroidization time of .25 microseconds. Assuming the greatest possible speed it could come off of the disk is the tangenial velocity of the disk edge, or 21.2m/s. Then the minimum travel distance before spheroidization is about 5 microns. This means that a droplet of this size is non-spherical due secondary atomization as the particles in this size range had adequate time and distance to spheroidize.

After attempt number one was complete the disk diameter was lowered from 2in to 1.7in in order to affect the mean particle diameter (Eqn. 1), as well as increase the particles flight time before striking the bath. The tangential velocity at the edge of the disk should be lower (18m/s), lowering droplet speed as well as a small increase in flight distance from the edge of the disk to the oil. Further, the superheat applied to the melt before pouring was decreased

(Table 1), ideally allowing the particles to begin solidification before impinging on the oil bath.

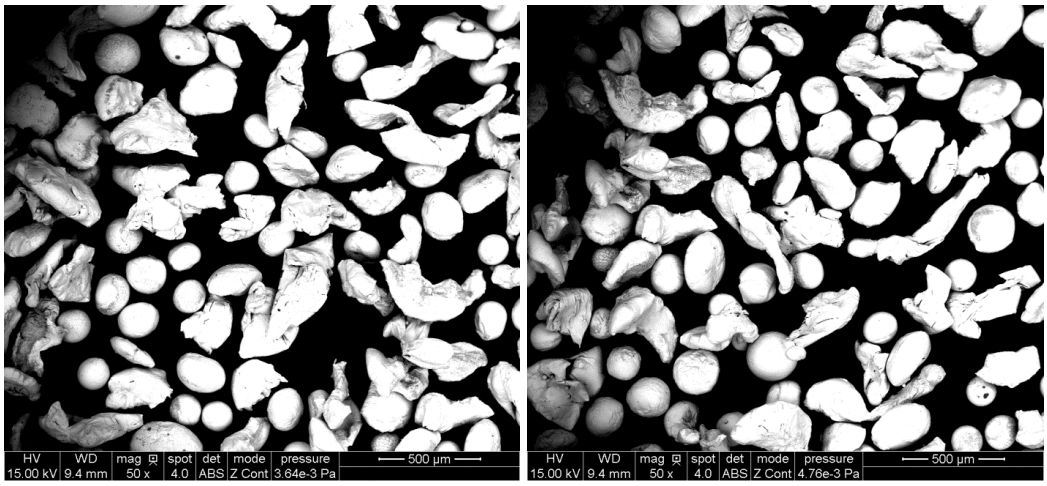

Figure 12: RDA-2 gadolinium powder image (150-250µm) sieve

These changes increased the amount of spherical powder present in the desired size cut (Fig. 12). However, many irregular particles exist in this size hampering the usefulness of this powder. In the size ranges above and below the 150-250µm cut (see Fig. 13) there are mostly spherical powders in the lower size range and mostly flakes in the upper size range.

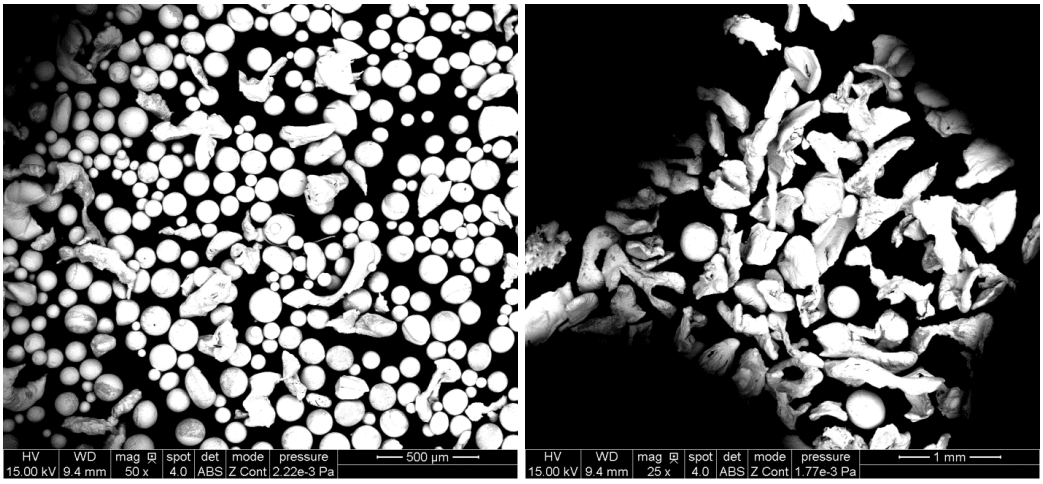

Figure 13: RDA-2 gadolinium powder image (45-150µm left, 250-425µm right)

This suggests a cut off of droplet sizes where smaller droplets at least partially solidify before impinging on the oil bath or wall due to their larger cooling rate and shorter

solidification time, and larger particles are deformed on impact [23]. A lower superheat of 95°C was desired for the third run of pure Gd in order to make the powders produced more spherical.

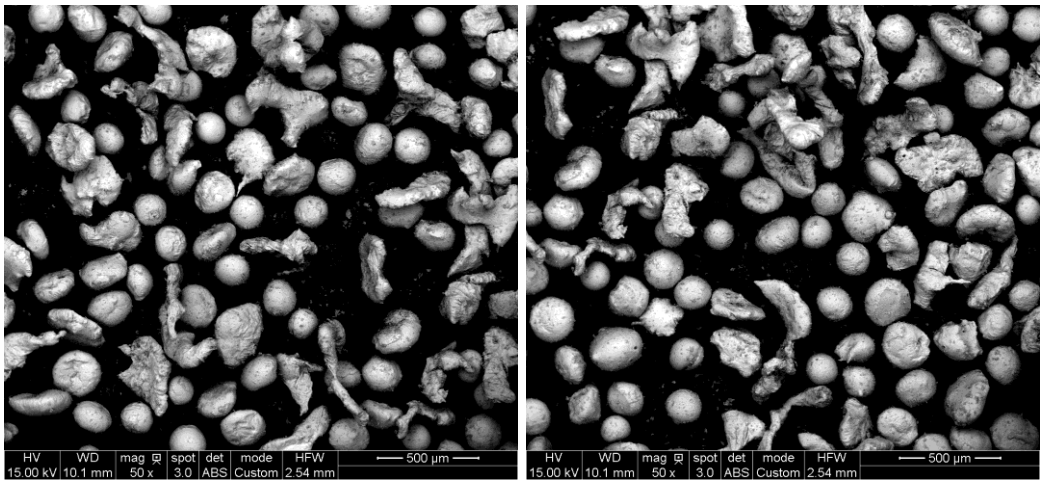

Figure 14: RDA-3 gadolinium powder image (150-250µm)

The decrease in superheat for the third run further improved the powder morphology (Fig. 14), however many flakes are still present in the powder. The superheat of the melt is one of the key factors in controlling powder morphology in powders created using this quench bath method. Decreasing the superheat further was not attempted because in the RDA-3 atomization, near the end of the run a skull formed on the disk. Skull formation happens in each run however in the RDA-3 run a larger, unbalanced skull developed (figure 15 and 16).

Figure 15: Skull Developed on RDA-3 disk

Figure 16: Typical RDA skull

This type of skull puts stress on the atomization shaft and motor and in this case bent the shaft. This puts a practical limit on the superheat that can be applied to the melt. It is important to note that after the stopper rod is lifted the temperature of the melt can no longer be accurately measured although the run is very short (30-60s).

Gadolinium-Yttrium

The second alloy in this study is a binary alloy $Gd_{.91}Y_{.09}$ at% alloy. These elements exhibit total solubility with one another (Fig. 17). This allows for a continuous curve of magnetic properties from pure gadolinium to pure yttrium [31].

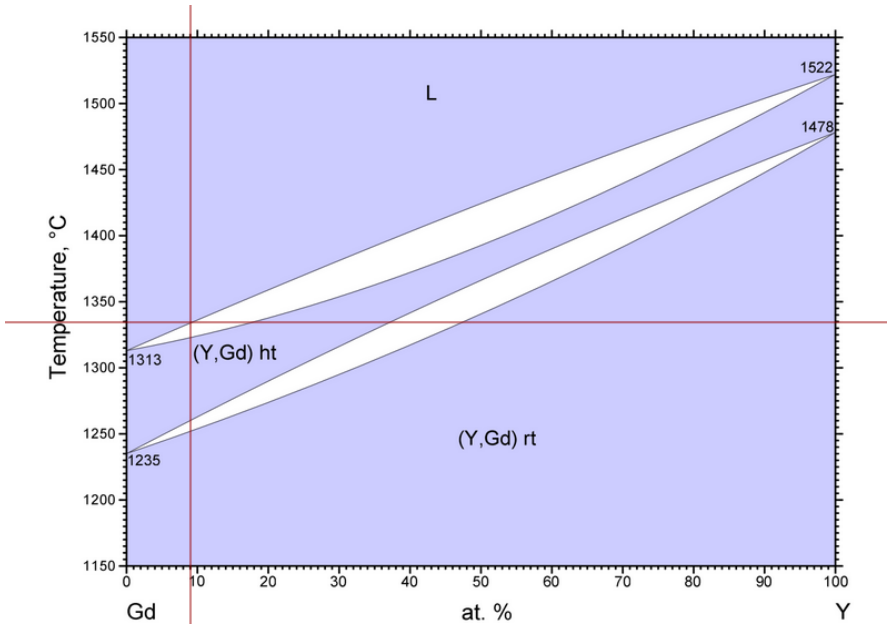

Figure 17: Gadolinium Yttrium phase diagram with alloy composition marked [24]

By alloying with yttrium the Curie temperature of the alloy can be adjusted. In this case yttrium causes a depression in the Curie temperature of the alloy making this alloy a natural follow up to pure gadolinium [31]. The alloy charge in these runs is fully arc melted commercial purity gadolinium and yttrium to attain the correct stoichiometry. This alloy has an increased melting temperature compared to pure gadolinium so the pour temperature was higher compared to RDA-3, but the superheat was attempted to be kept the same in either case. All other atomizer settings were kept constant compared to RDA-3 (Table 1).

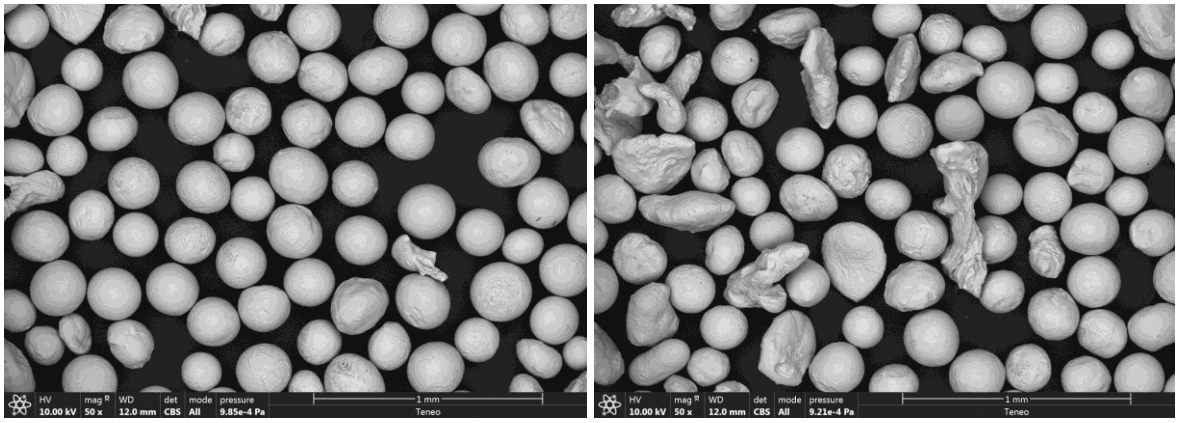

Figure 18: RDA-4 Gd-Y powder image (150-250µm)

The RDA-4 powder is the most spherical of all the previously made powders (Fig. 18, 19). This is likely due to the liquid properties of the melt. Pure liquid yttrium does not have a significantly larger surface energy than gadolinium [25]. However, their melting points are far apart and no experimental data could be found on the surface energy of this alloy.

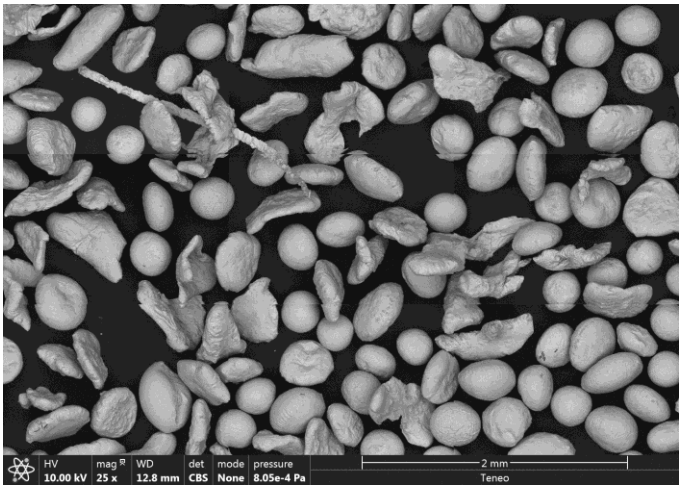

Figure 19: RDA-4 Gd-Y powder image (250-355µm)

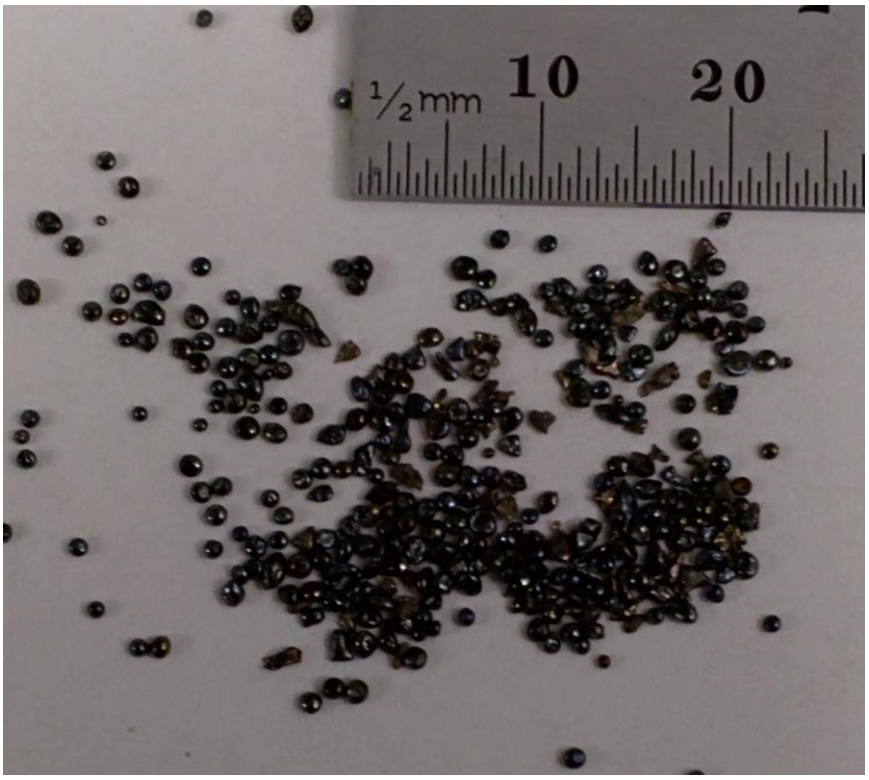

Figure 20: RDA-4 photo of particles >500µm

In stark contrast to the pure gadolinium powder this alloy had spherical particles that were larger than 500µm (Fig. 20). This indicates a significant change in the liquid properties and not a change in the operation of the atomizer. A few large particles of pure gadolinium were produced in the previous runs, but they did not remain spherical after solidification.

Equation 1 worked well for the pure gadolinium case and the GdY liquid properties were unknown, it was used to attempt to calculate ideal parameters for RDA-5 based on the measured d_{50} of RDA-4. The variations in atomization parameters made from RDA-4 to RDA-5 were increasing the disk diameter and the disk speed to attempt to obtain a finer size distribution. Increasing the disk diameter to 2 in from 1.7 in and inputting the desired d_{50} of 200 microns compared to the measured d_{50} of RDA-4 allowed the disk speed to be calculated at 19,290rpm using Eqn. 1.

During RDA-5 a sound was heard that was abnormal to the atomizer and the disk and coil were turned off around 30s into the run to protect equipment from damage. The tantalum disk had come detached from the apparatus. Some remaining melt poured onto the stationary disk and the run froze out. There was several hundred grams of powder that made it into the bath, but this run was incomplete.

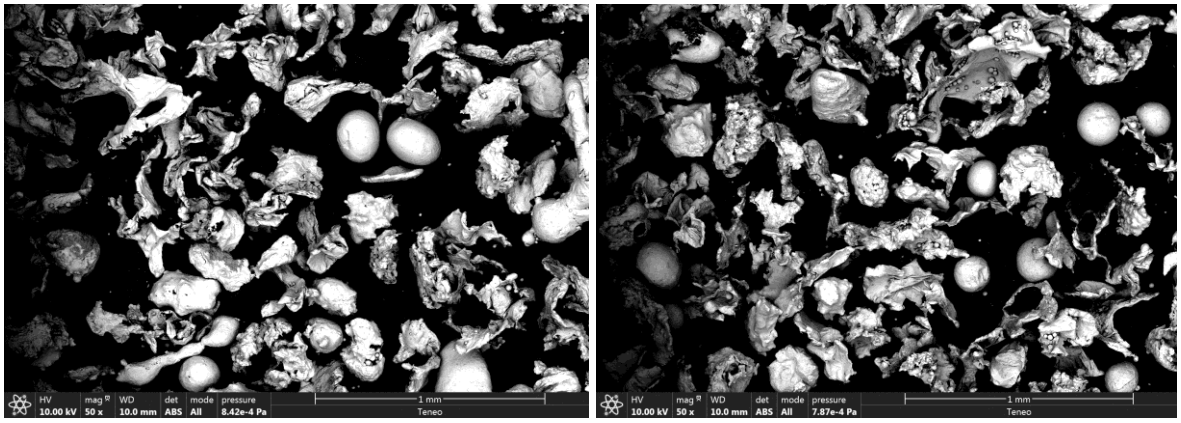

Figure 21: RDA-5 GdY powder image (150-250µm)

The powder in the 150-250µm size range for RDA-5 contains very few spheres and once again the powders are mainly flakes (Fig. 21). This likely stems from the increase in disk diameter and disk speed that was used for the run. The tangential velocity of the disk in this run compared to the previous runs is more than double (50.8m/s). This would have two effects on the droplet coming from the edge of the disk. One is that the flight time from the disk to the bath could be more than halved for a droplet that is flung from the disk. The other effect is the larger force of the impact with the liquid bath which could even cause the droplet to hit the quench bath wall. Both of these effects make it more likely that a droplet flung from this disk will not have time to solidify before striking the bath and make it less likely for a droplet to remain spherical after striking the bath.

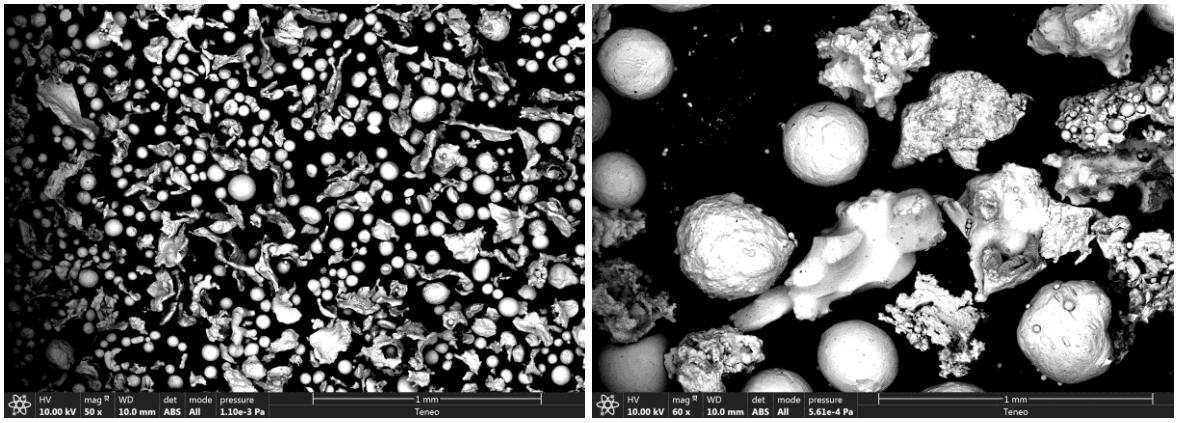

Figure 22: RDA-5 GdY images (45-150µm left, 250-355µm right)

Particles that were finer than the target size range in this case tended to be more spherical than the target size range (Fig. 22). This is likely due to the more rapid solidification that occurs in the finer particles allowing them to be solid or at least partially solid before striking the bath. In this case, the particles that were larger than 250 microns also tended to be more spherical than the particles in the 150-250 micron range.

Powder Bed Packing

An important property of the powder that is tied to the powder morphology is how well the powder will pack in a powder bed, which can be quantified by powder porosity. The amount of powders able to pack in a given volume is directly tied to the efficiency of the refrigerator. The packing is directly related to the mass of powder that can be affected by the magnetic field applied to it. For this project the goal was to achieve 36% porosity or lower at maximum powder packing. This is calculated by measuring the volume of a known mass of powder, then using tapping and vibration to make the powder volume as low as possible. The density of the powder is then compared to the fully dense material (Table 2 below).

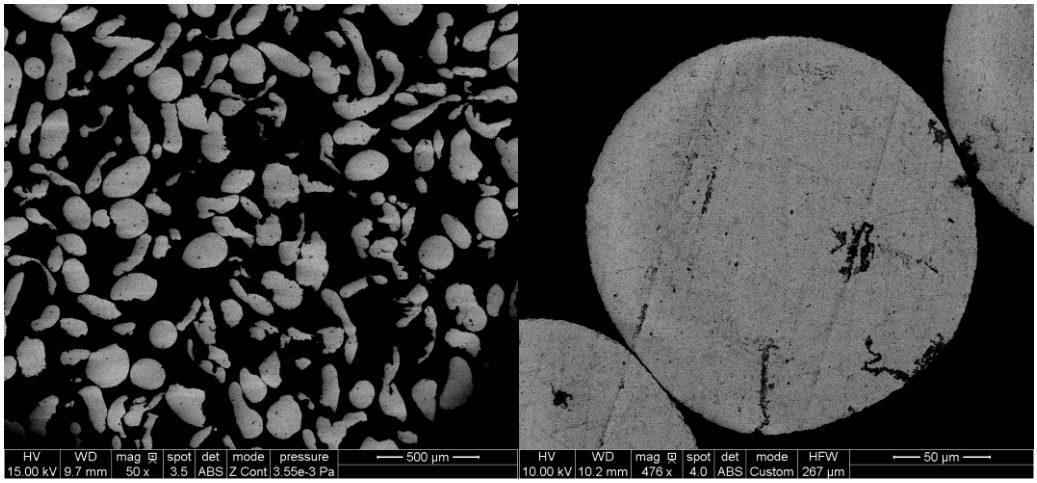

Figure 23: Cross sectioned 150-250µm powder(RDA-1 left, RDA-2 right)

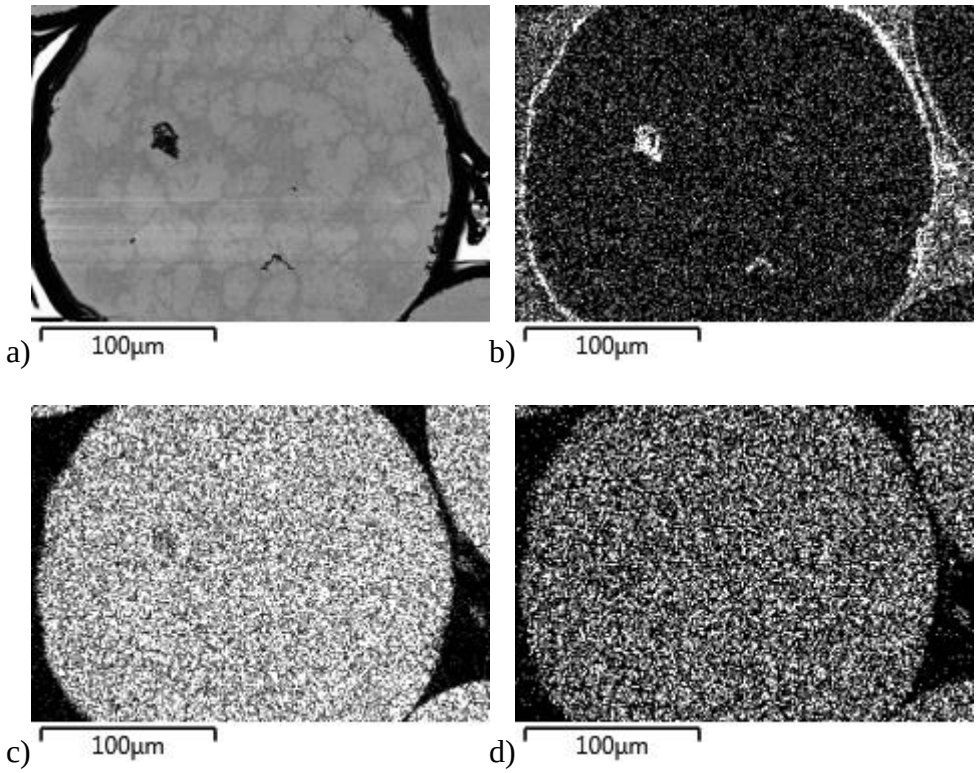

Figure 24: EDS map of a cross sectioned RDA-4 particle a)=the original image, b)=O, c)=Gd, d)=Y)

These images illustrate the lack of internal porosity in the powders (Fig. 23, 24). The dark parts of the images are internal oxides (confirmed by EDS). The lack of internal pores is an advantage of centrifugal atomization. However, in this study the amount of flakes in the as

produced powder were too high to achieve reasonable packing. Therefore, it was necessary to "deflake" the powder before it is usable (Fig. 25).

Deflaking was achieved via rolling the particles along a tilted, flat surface and collecting the particles that rolled to the bottom, periodically removing the particles stuck to the surface.

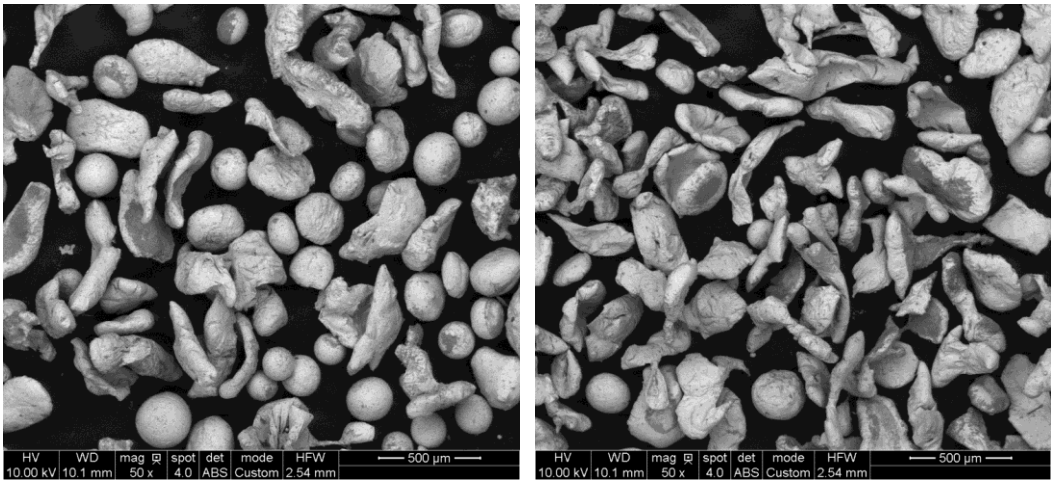

Figure 25: Example of deflaking process RDA-2 (deflake left, flakes right)

The process is not perfect but after several attempts the powder had a larger packing density (Table 2).

Table 2: Porosity % of fully packed powders

Material	Porosity %
RDA-2 150-250µm De-Flake	46%
RDA-3 150-250µm De-Flake	42%
RDA-3 150-250µm Flake	54%
RDA-3 45-150 As Sieved	41%
RDA-4 150-250 As Sieved	39%
RDA-5 150-250 As Sieved	64%

With more deflaking runs on the particles the density may approach the desired 36%, but the total mass of powder was also decreasing due to the flake separation. Another possible way to decrease porosity is to decrease contamination of carbon and oxygen in the final powder as the oxides shown are less dense than the material and also detract from magnetic properties. It was decided that this porosity was acceptable to begin testing the powders in the refrigerator. Worth noting is that the improvement in powder morphology corresponds with greater packing densities. The packing improved with each run until RDA-5.

CHAPTER 4

POWDER YIELD

Gadolinium

An important consideration for atomization is the powder yield since the raw material is expensive. As noted above the effective yield in this case depends on two factors, one being particle size and the other particle morphology. From Eqn. 1 and using values for pure liquid gadolinium the estimated d_{50} for RDA-1 is 176µm and for the other runs of pure gadolinium it is 193µm. This is due to the reduction of disk diameter from 2 inches to 1.7 inches between the runs. It is also important to note that the melt flow rate of the liquid is not constant as the crucible is gravity fed. The melt flow is the highest at the beginning of the run and the lowest at the end of the run but for the calculation was treated as constant.

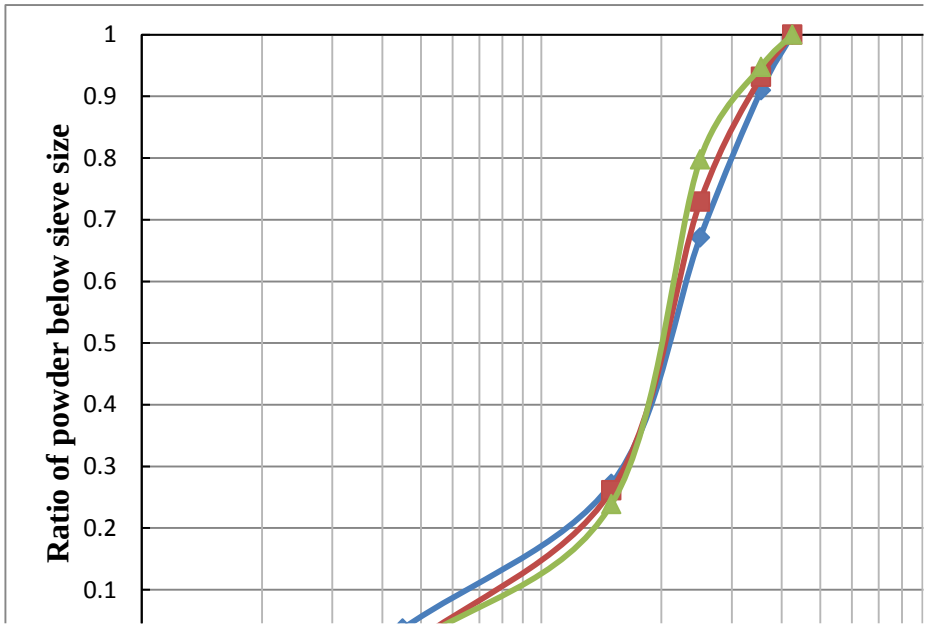

Figure 26: Particle size distribution from sieve for pure Gd

As can be seen in figure 26, at the low end of the distribution RDA-1 produced finer particulate compared to the other runs, as predicted. However the prediction falls apart at the

desired size range and above. This is due to the particle morphology and how the particulate pass through the screens which are influenced by their morphology (Fig. 27, 11). In RDA-1 there were very few spheres in the 150-250µm size range. In fact the particle shapes were largely irregular.

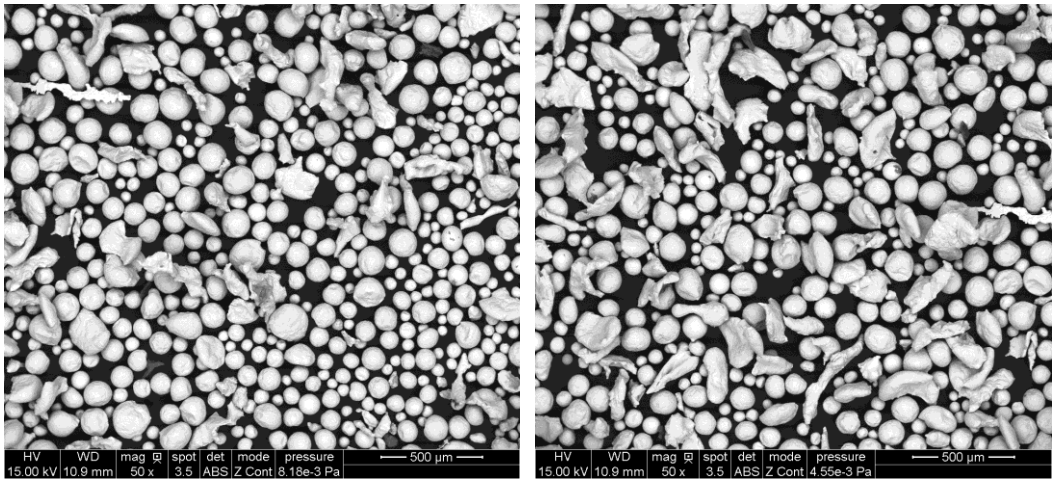

Figure 27: RDA-1 gadolinium powder image (45-150µm)

Since the prediction was based on REP atomization which produced very spherical powders [13], the prediction will not hold for powders that do not interact with the screens the same way. For instance, flake shape powders may not pass through a screen which they otherwise would have if they were spherical. On the other hand ligament shape powders, or powder with large aspect ratios will pass through a screen they would not pass through if they were spheres.

Table 3: d_{50} and standard deviation of gadolinium runs

Run	Sieve d_{50} (µm)	Sieve d_{84}/d_{50}	Microtrac d_{50} (µm)	Microtrac s.d. (µm)
RDA-1	212	1.53	-	-
RDA-2	205	1.46	247	179.8
RDA-3	200	1.33	237.4	167.2

The particle size distributions (Table 3) for RDA-2 and RDA-3 both are very similar. RDA-3 has a lower d_{50} and the distribution is tighter this is once again due to the more spherical shape of the powder. The differences between the run were superheat and charge mass.

In the more spherical runs of RDA-2 and RDA-3 the prediction of the d_{50} from equation 1 is very similar to the actual results.

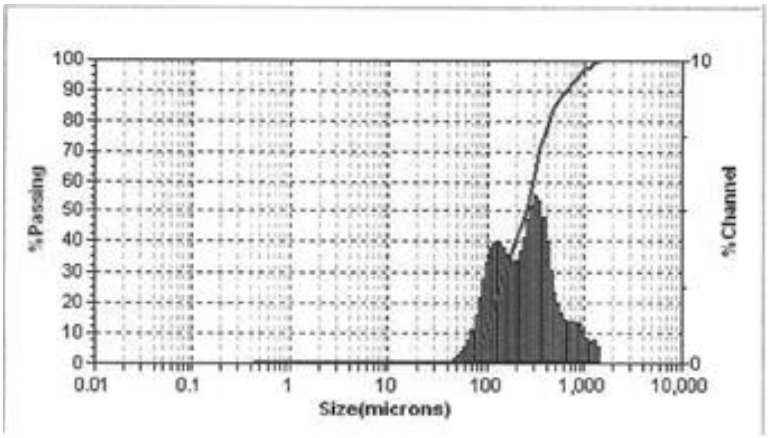

Figure 28: Microtrac plot of RDA-2

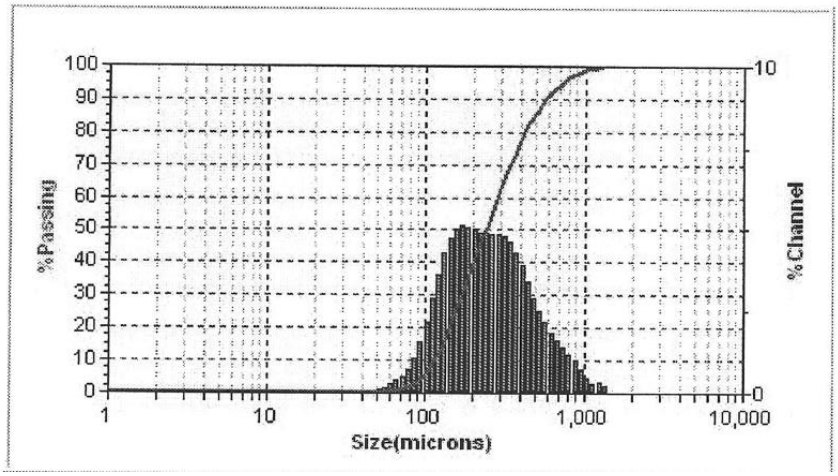

Figure 29: Microtrac plot of RDA-3

The microtrac data show typical particle size distributions for centrifugal atomization experiments operating in the ligament formation mode [13]. These bimodal distributions illustrate the coarser primary droplets and the finer secondary droplets (Fig. 28, 29).

The microtrac method always shows a coarser d_{50} than the sieve size method likely due to particles with high aspect ratio that would pass through a screen but be measured with laser diffraction as a large particle.

It is apparent that the yield is dependent on liquid properties as well as machine parameters, however interaction with the oil is one of the most important parameters and this comes from the superheat of the powder.

Gadolinium-yttrium

Although the powder morphology for RDA-4 is superior to the prior runs, the powder yield is small due to the particle size distribution (Table 4). Since no experimental liquid surface tension data is available on the Gd-Y alloy, the predictions from Eqn. 1 have limited use. Eqn. 1 was also derived from atomization of pure metals. In order to get an idea of parameters to use for this run the liquid density was calculated and a crude predictor of the

rule of mixing between the surface tension of pure gadolinium and pure yttrium liquid was used. The equation predicted a d_{50} of 195µm using the same parameters as the RDA-3 run. The prediction was not particularly close despite the fact that the powders were largely spherical even above 500µm (Fig. 30).

Table 4: d_{50} and standard deviation of GDY runs

Run	Sieve d_{50} (µm)	Sieve d_{84}/d_{50}	Microtrac d_{50} (µm)	Microtrac s.d. (µm)
RDA-4	530	1.77	-	-
RDA-5	93	3.76	96	62.9

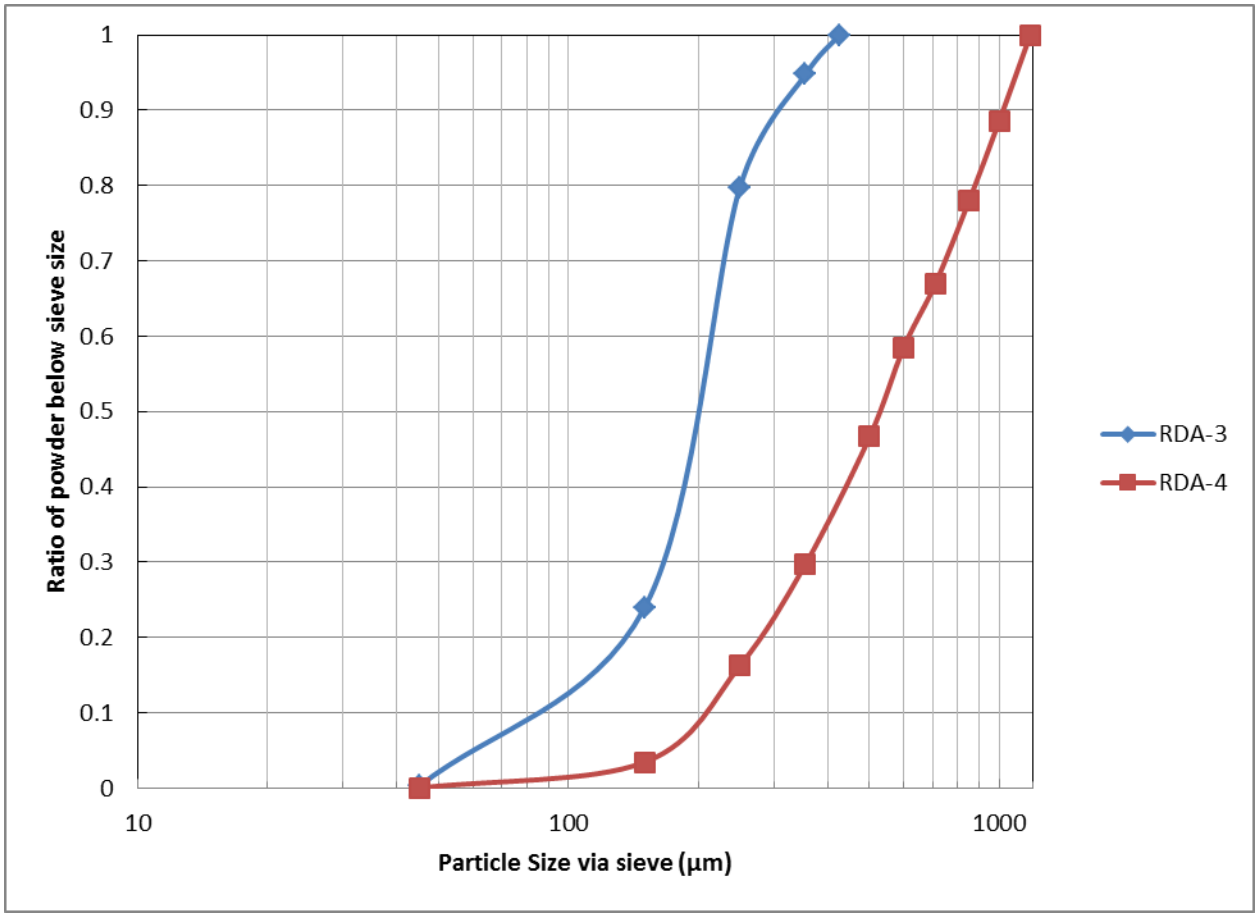

Figure 30: Powder size distributions of gadolinium compared to GD-Y with identical run parameters

After the disk speed was calculated by equation 1, the run RDA-5 was performed. It is worth noting that the run was not fully complete before the disk failed and the run had to be terminated as described above.

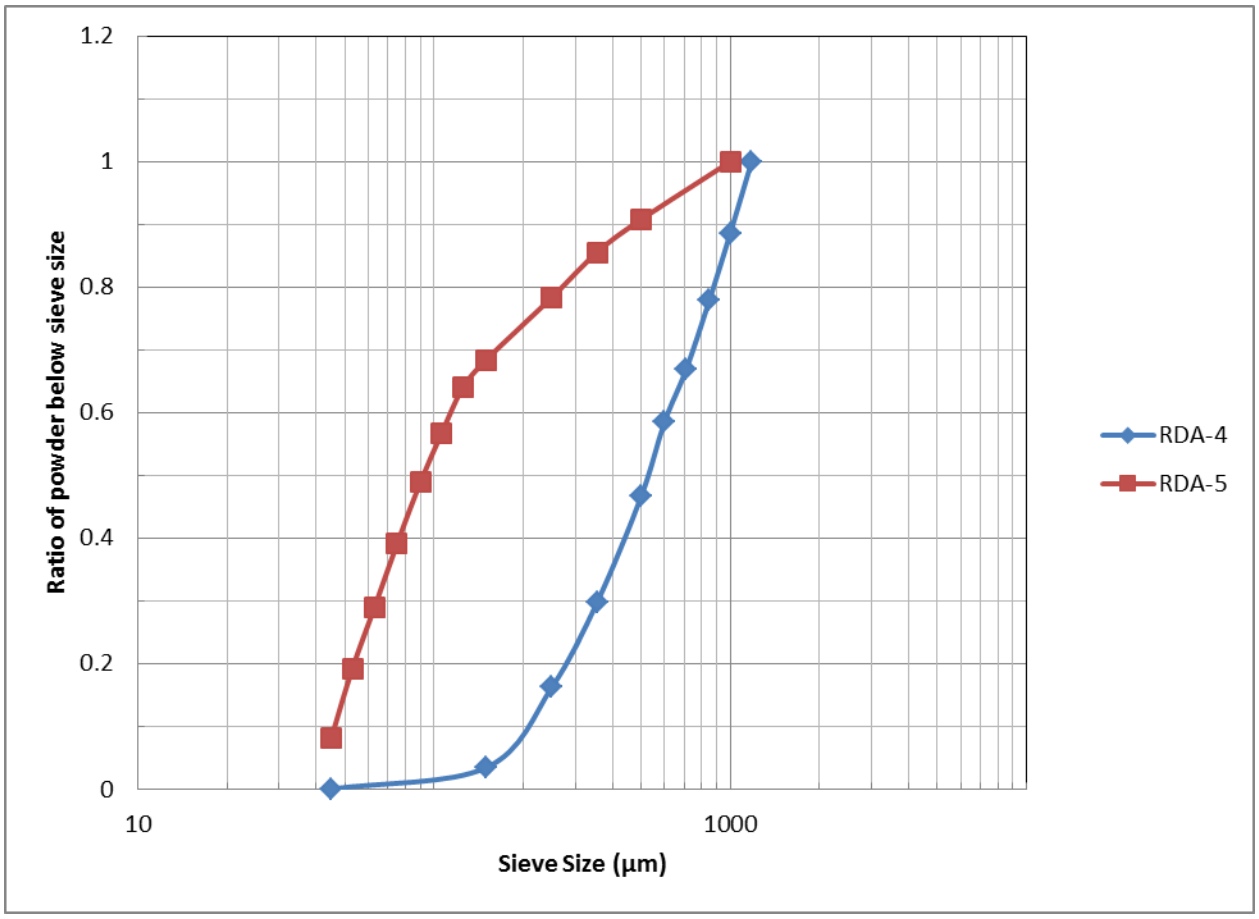

Figure 31: Particle size distribution with increase in disk rpm and diameter

As expected the particle size distribution was much finer than the distribution for RDA-4 (Fig. 31). However, the d_{50} of this distribution was much lower than even predicted. This calls into question the predictive ability for Eqn. 1 for this type of alloy.

Of the parameters in Eqn. 1 the only unknown parameter for the GdY alloy is the surface tension. In order to achieve the d_{50} found for RDA-4 the surface tension would have

to be 7.4N/m. More likely is that viscosity is coming into effect which is not accounted for in this empirical equation. The viscosity of this melt could be very high in the large mushy zone for this alloy.

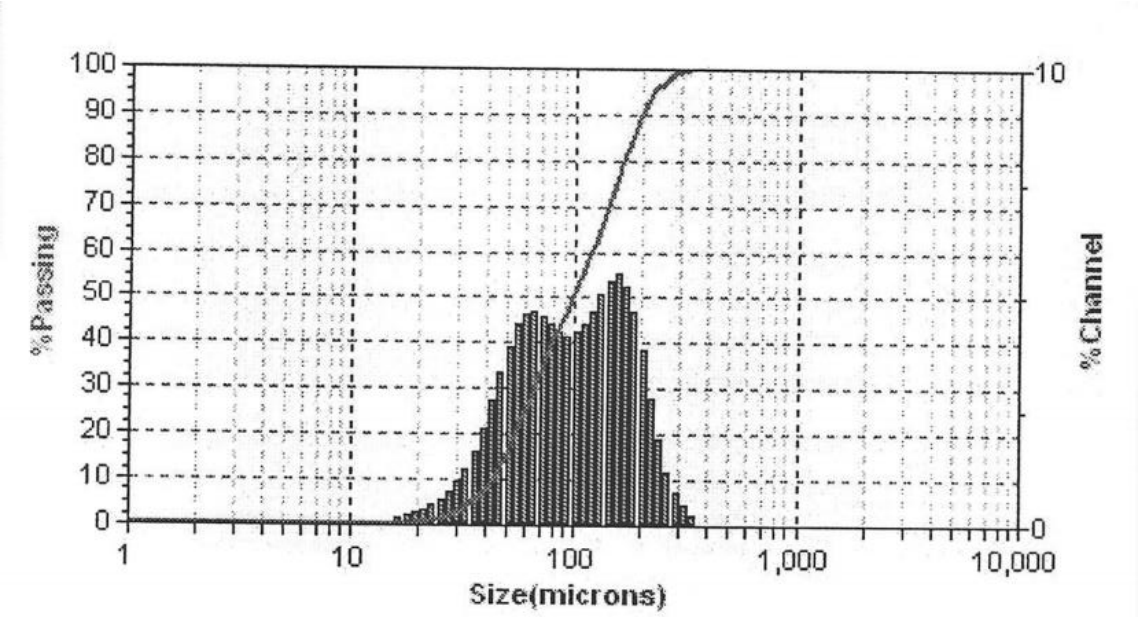

Figure 32: Microtrac of RDA-5

Disk Geometry

An important consideration to powder yield is the geometry of the disk. For the RDA-4 run high speed video was taken of the stream as it impacted the disk. Initially the disk design used was design b. from Figure 7.

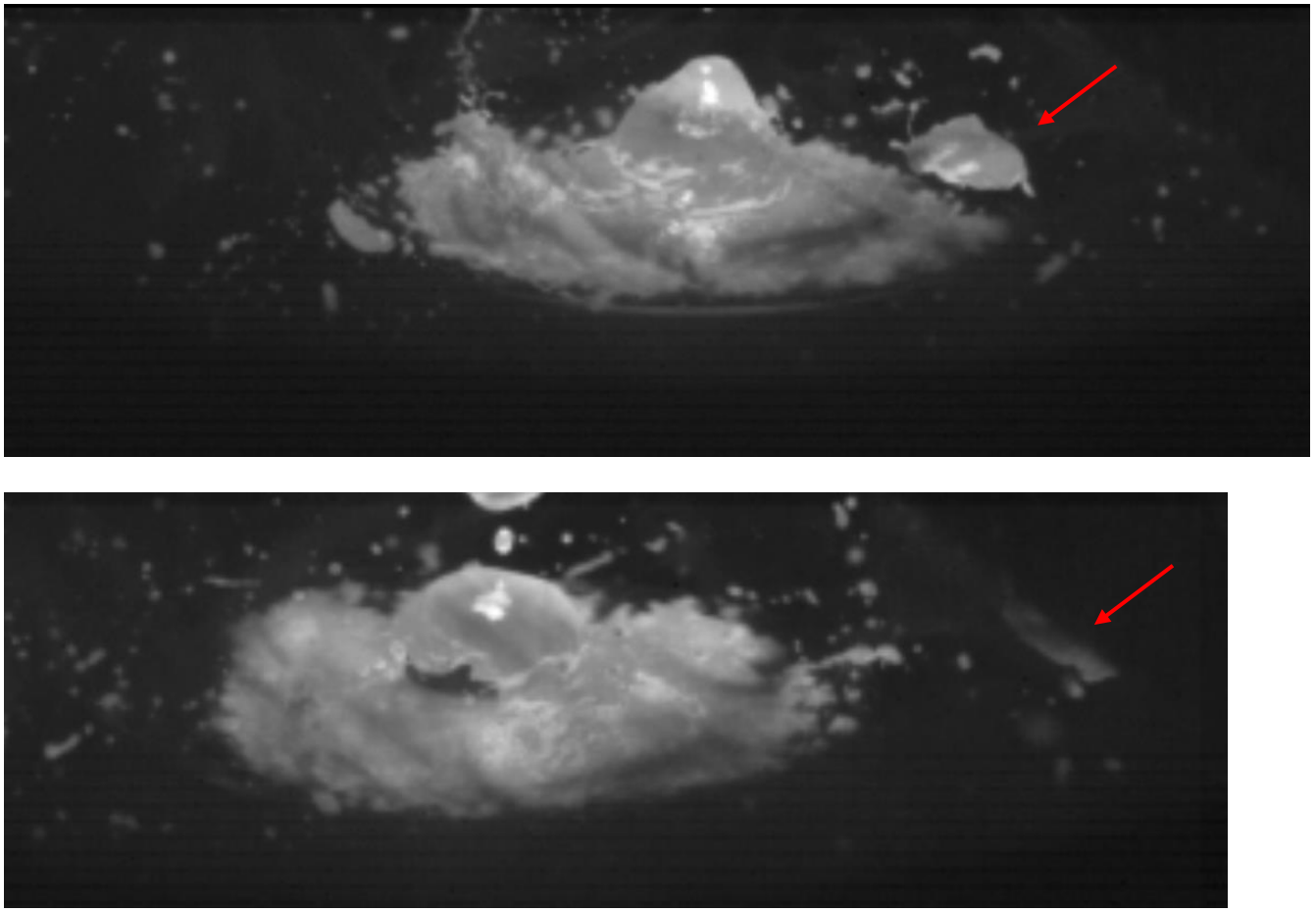

Figure 33: RDA-4 High speed video frames taken close together

As can be seen from this disk configuration the hemispherical part of the disk where the liquid is supposed to impact creates and sheds small skulls indicated by the red arrow in figure 33. This is accompanied by “splashing” of the liquid melt around the nub causing larger droplets to be formed that do not come from the edge of the disk as intended. This prompted the trial of design a from figure 5 which was designed so that the edge of the disk is higher vertically than the center. In addition, the shape of the center of the disk was changed so that wetting would still occur without splashing.

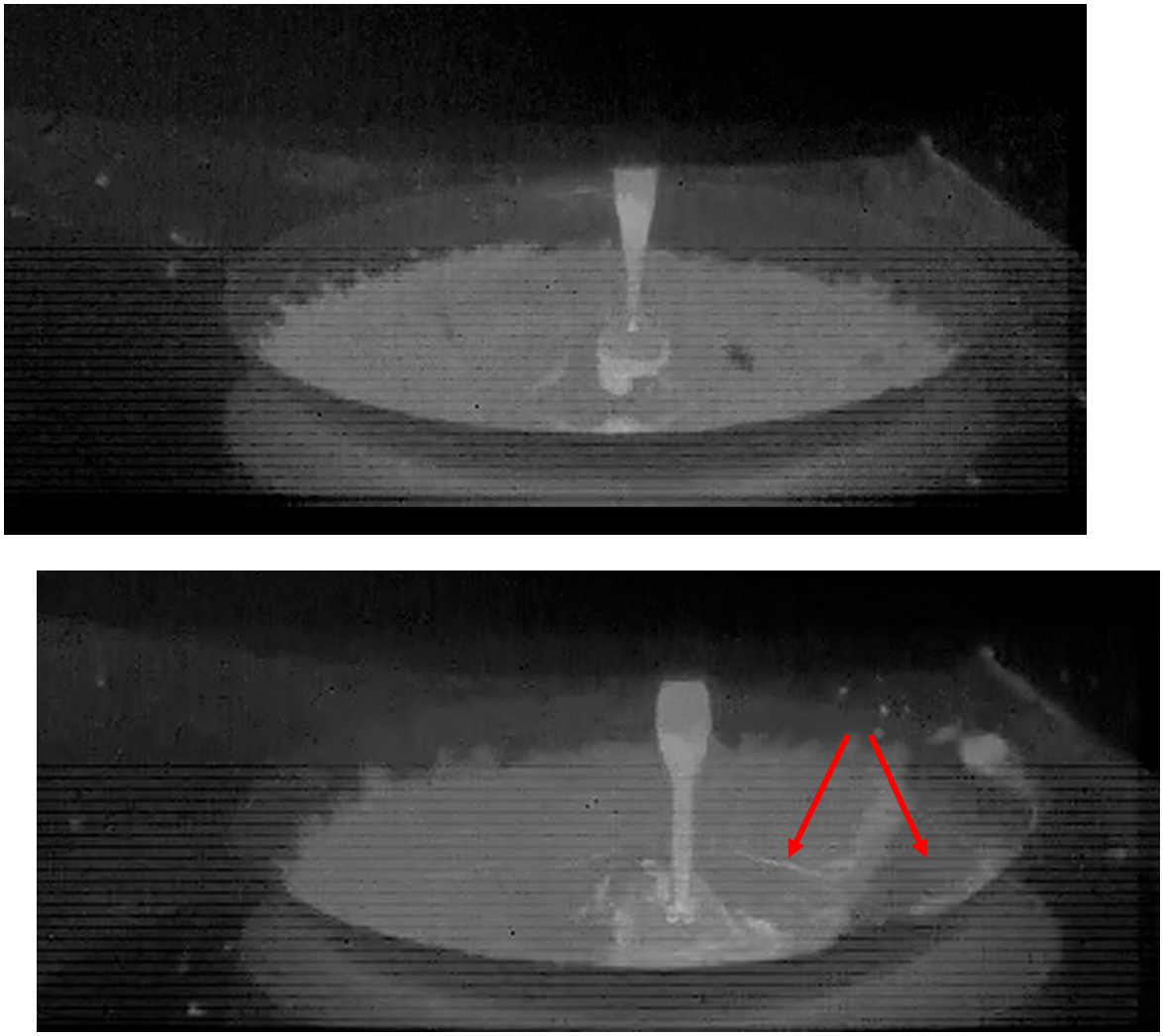

Figure 34: RDA-5 high speed video frames taken close together

The second disk design chosen appeared to have a more controlled atomization as most droplets were coming from the edge of the disk (Fig. 35), however early in the atomization a skull was shed from the disk (red arrows point to fracture of skull and skull missing). This skull when flung hit the edge of the disk and the disk deformed causing the disk to wobble (Fig. 34).

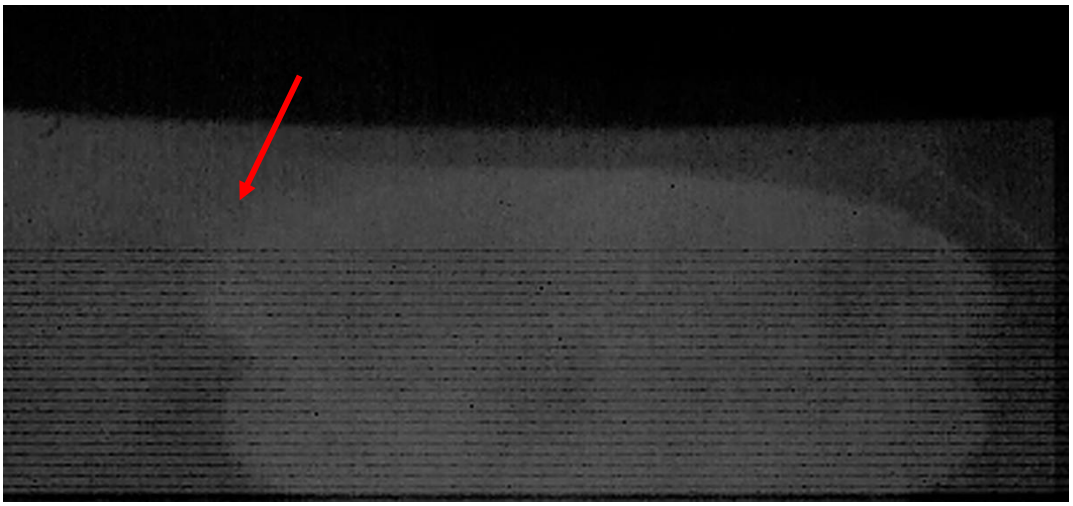

Figure 35: RDA-5 atomization spray

Unfortunately, some oil got onto the inside of the viewing window during the run, but later in the run a spray of metal can be seen coming from the edge of the disk despite the wobble in the disk. Further, the entire surface of the disk is wet with liquid metal. This design ultimately failed, as during the run (not captured on video) the disk detached from the apparatus. However, there appears to be some merit to having the edge of the disk being higher than the center for more uniform atomization [18].

CHAPTER 5

POWDER CHEMISTRY

Gadolinium

Powder chemistry is directly related to the Curie temperature and magnetization of the material. If carbides or oxides are formed within the powders the magnetic properties can decline. This decreases the efficiency of the final refrigerator. One important consideration on powder chemistry for this work is the composition of the charge material. In RDA-1 the charge material was gadolinium that had previously been processed via PREP. In RDA-2 and RDA-3 the charge was commercial gadolinium purchased from HEFA.

Table 5: Gd Carbon, oxygen, and nitrogen results measure by LECO wt% (150-250µm)

Run	Carbon ppm	Oxygen ppm	Nitrogen ppm
RDA-1 charge	497	1800	394
RDA-1	1280	9600	417
Difference from charge	783	7800	23
HEFA Gd	67	807	233
RDA-2	1030	3870	285
Difference from charge	963	3063	52
RDA-3	1200	1600	267
Difference from charge	1133	793	34

The particles pick up carbon, oxygen, and nitrogen in all cases during the atomization event (Table 5). There are several possible sources of contamination that occur during the process including atmosphere, crucible contact, disk contact and contamination from the oil itself.

In the case of RDA-1 an important source of contamination was the crucible itself. The crucible used in this case was Yttria lined YSZ made by arc spraying. It was thought that Yttrium would be able to contain the electropositive gadolinium (Fig. 36). After the atomization run the powder was cross sectioned and imaged. EDS detected ~5at% yttrium in the powder.

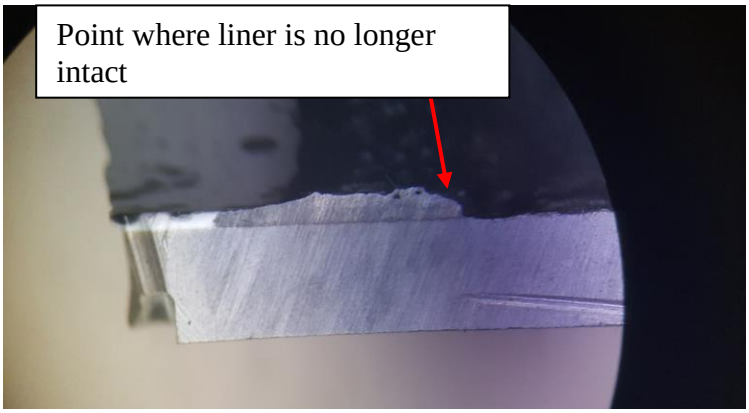

Figure 36: Crucible liner erosion

The presence of yttrium also suggests that an increase of oxygen also took place in the material as the yttrium was not present as an oxide. In order for yttrium metal to be present in the material an oxidation-reduction reaction must have occurred and the LECO analysis supports this.

RDA-2 and RDA-3 were processed in tantalum in order to prevent this type of contamination. The analysis of these two runs shows no elemental contamination on EDS scans aside from oxygen and carbon. The small nitrogen pickup in all cases indicates that contamination is not largely coming from the atmosphere in the atomization chamber. The bulk of the impurity pick up likely comes from the quenching oil. Although the oil is silicone based and more stable than hydrocarbon quench oils, during the atomization run smoke or steam is emitted from the oil. Further, the oil changes to a darker color after the run are

complete. The oil is not reused between runs. This suggests that a lower superheat should cause less contamination from the oil. The carbon pickup appears to increase with a decreasing superheat, whereas the oxygen pickup decreases with decreasing superheat.

After each run the Tantalum crucible was etched with nitric acid in order to remove any excess gadolinium from the inside of the crucible and reused. Creating a tantalum crucible is somewhat costly and so it is important to note that on the second use of the crucible only the carbon pickup increased. It is not clear what the cause of this increase is, but it is important from a production standpoint that the tantalum crucible is able to be used for more than one run without introducing excessive contamination of the powder.

Gadolinium-yttrium

For the gadolinium yttrium runs the charge was arc melted prior to atomization due to the difference in melting temperature and density of the two metals this is intended to fully homogenize the charge prior to melting. Only the charge for RDA-5 was measured by LECO since it was assumed that the charges would be identical. Unfortunately, all of the charge for RDA-4 has been atomized so repeating these measurements is not possible.

Table 6: GdY Carbon Oxygen, and Nitrogen result measured by LECO wt% (150-250µm)

Run	C ppm	O ppm	N ppm
RDA-4	841	1770	444
RDA-5	1470	7620	403
RDA-5 charge	91	1970	326

It is likely that there was a variation in the charge between the two runs since it is unlikely that the amount of oxygen went down after the RDA-4 run (Table 6). However, it is important to note that the level of contamination is much higher in the RDA-5 run.

CHAPTER 6

MAGNETIC PROPERTIES

Gadolinium

The magnetic properties are important at determining the ultimate performance of the refrigerator. The properties were measured using a vibrating sample magnetometer [26]. The properties measured here are somewhat dependent on powder chemistry (Table 7).

Table 7: Saturation Magnetization of the materials at 10k

Material	Saturation Magnetization (emu/g)
RDA-1	232.2
RDA-2	265.6
RDA-3	268.4
RDA-4	231.8
RDA-5	246.1
RDA-1 charge	269
HEFA Gd (2,3 charge)	256
GdY arc melt (4,5 charge)	243.7

In the plot below from RDA-1, it can be seen that the magnetic properties of the charge vary greatly from the magnetic properties of the resulting powder. During the production RDA-1 in the yttria lined crucible it was noted that the powder picked up oxygen and yttrium from the crucible. The decrease in Curie temperature in this alloy means it will not be suitable for the application (Fig. 37).

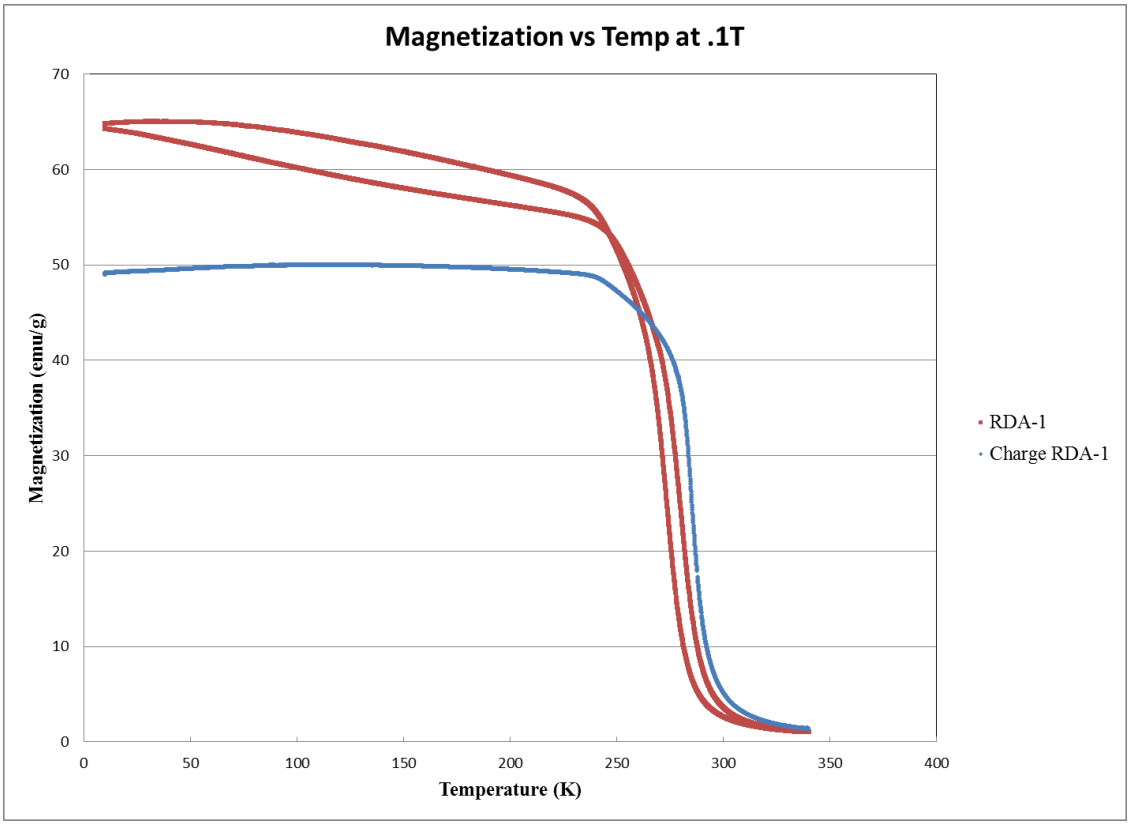

Figure 37: RDA-1 magnetic properties

Yttrium contamination not only affects the Curie temperature but it also lowers the saturation magnetization of the material. When saturation is lowered this means that there is less drop in magnetic entropy of the material when exposed to a magnetic field and that the material becomes less efficient as a magnetocaloric material (Fig. 38).

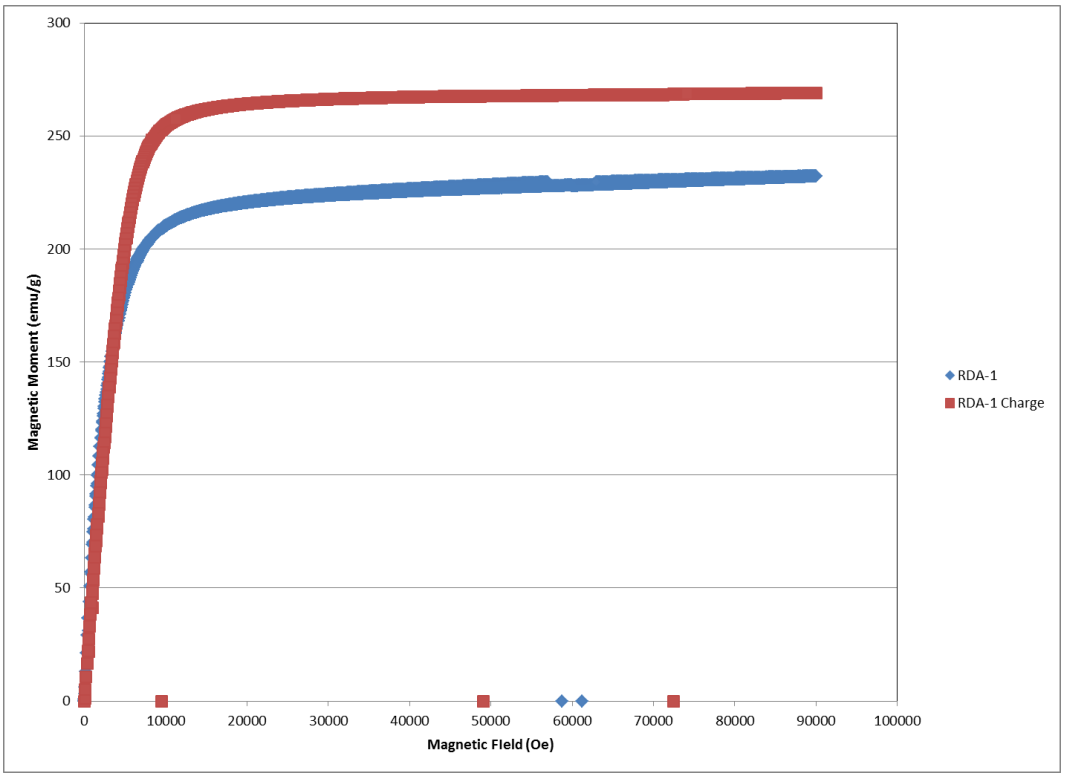

Figure 38: RDA-1 magnetic properties at 10k

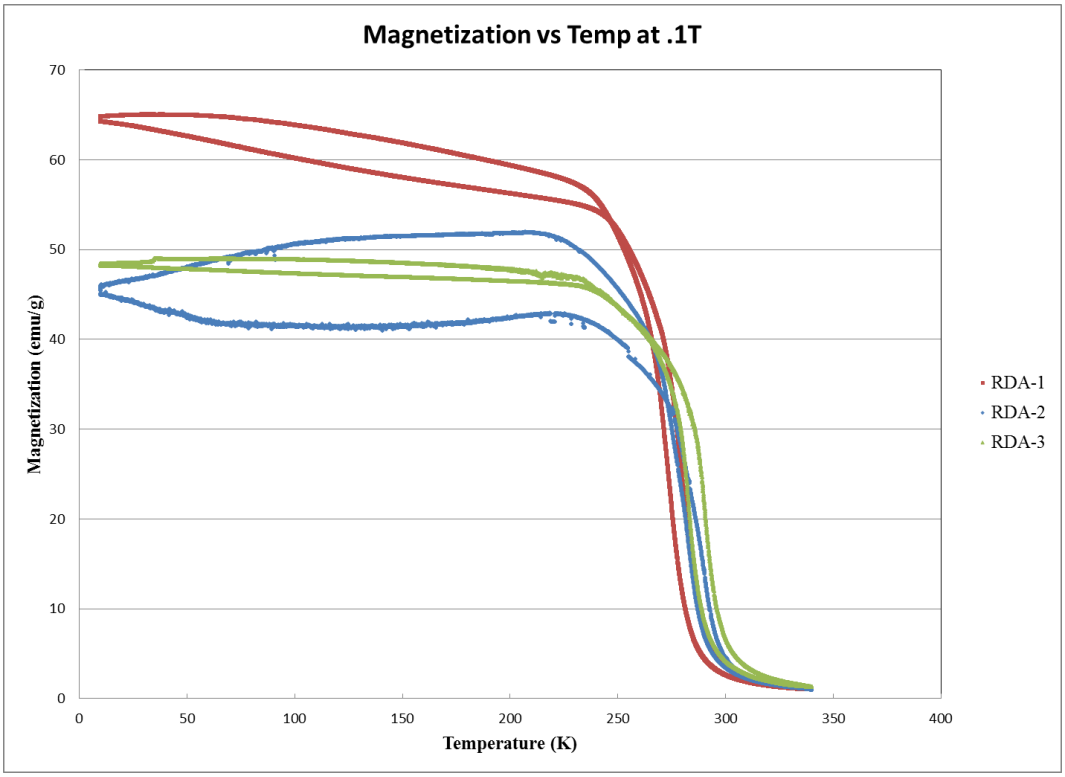

Figure 39: Comparison of gadolinium powders magnetic properties

As can be seen in figure 39 above, the Curie temperature for RDA-2 and RDA-3 is higher than that of RDA-1 by around 10°C. This is an indication of the lack of yttrium contamination that occurred in RDA-1 from switching to a tantalum crucible.

For RDA-2 and RDA-3 the Curie temperature as measured is basically unchanged between the charge material and the atomized powder. However the saturation magnetization is slightly higher in the powder compared to the charge material. There could be several explanations including the high temperature phase of Gd quenched into the powders, a change in properties from the oxygen and carbon pickup, but most likely this comes form the calcium present in the charge being outgassed during melting. It is important to note that the saturation magnetization of the charge as well as the powder material agrees well with literature values indicating that this is a good processing technique to produce effective gadolinium powders [28].

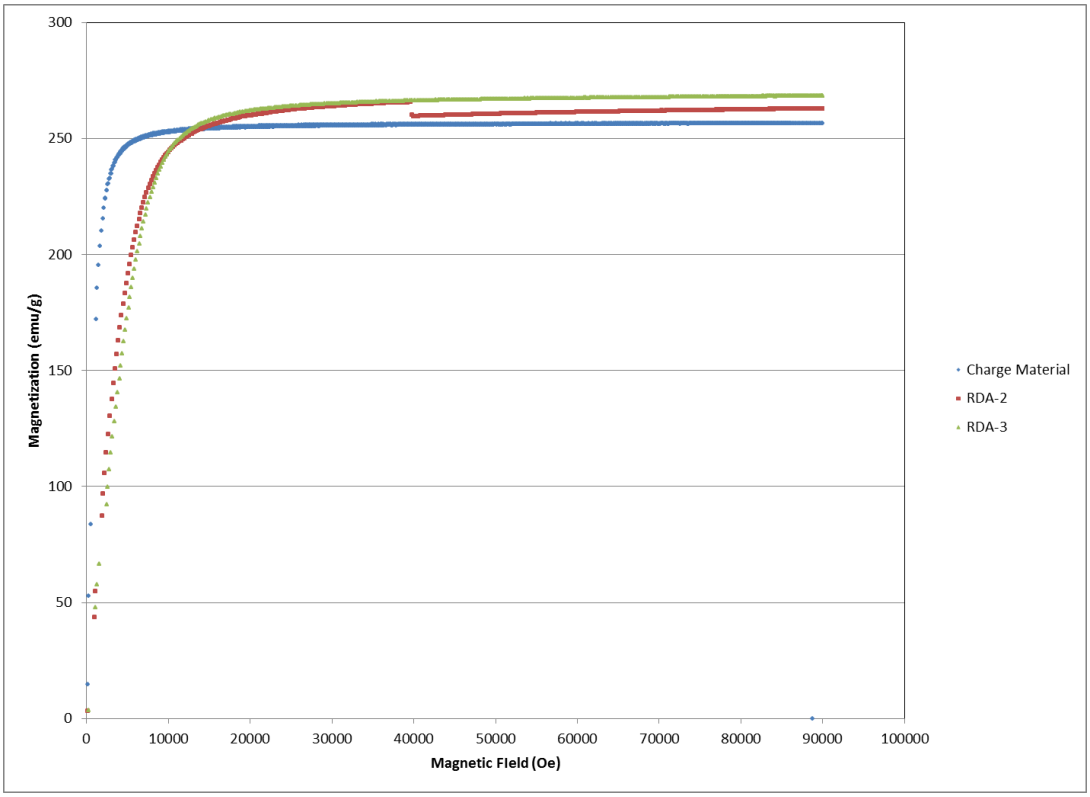

Figure 40: RDA-2 and RDA-3 magnetic properties at 10K

The magnetic saturation of the atomized materials also increased with decreasing superheat during the atomization run. This is likely due to the decreased oxygen contamination picked up from the oil (Fig. 40).

Gadolinium-yttrium

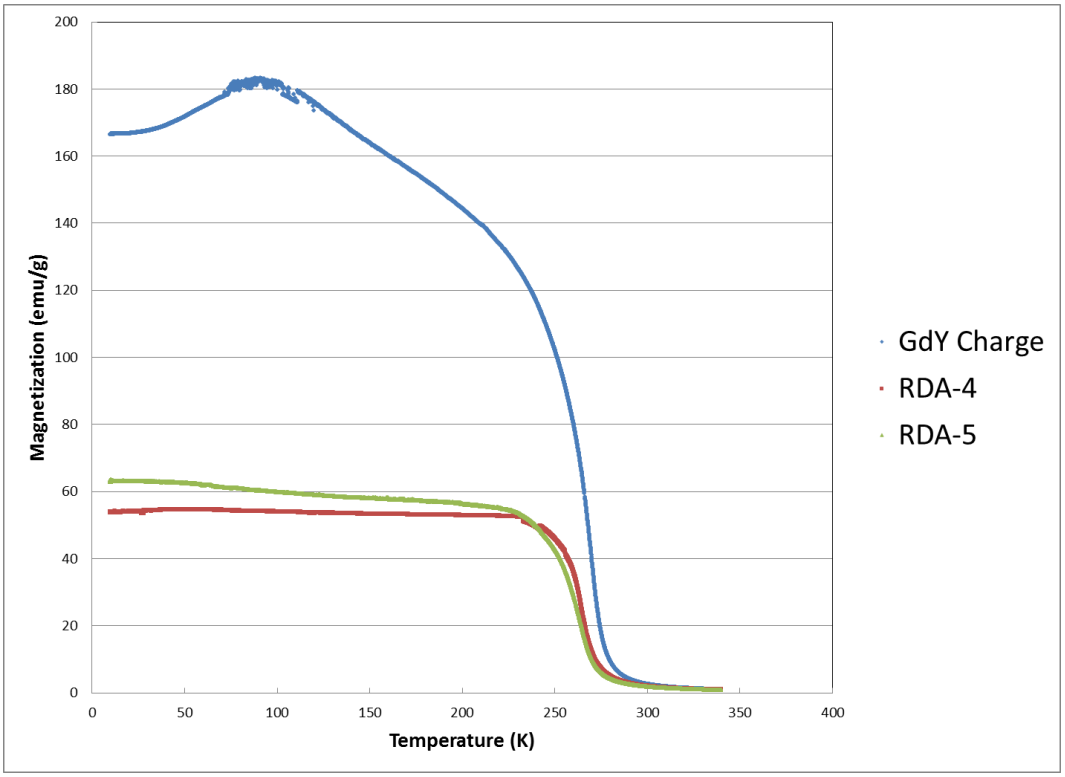

Figure 41: RDA-4 and RDA-5 magnetic properties

In the gadolinium yttrium runs the powders themselves have very similar Curie temperatures which match the Curie temperature expected by the models. However, the charge for RDA-5 has a higher Curie temperature than the powder as well as the Curie temperature predicted and measured for the drop cast alloy of the same composition (Fig. 41). As mentioned earlier the charge may not have behaved the same for RDA-4 and RDA-5 despite the same starting materials being used and both charges being fully arc melted together.

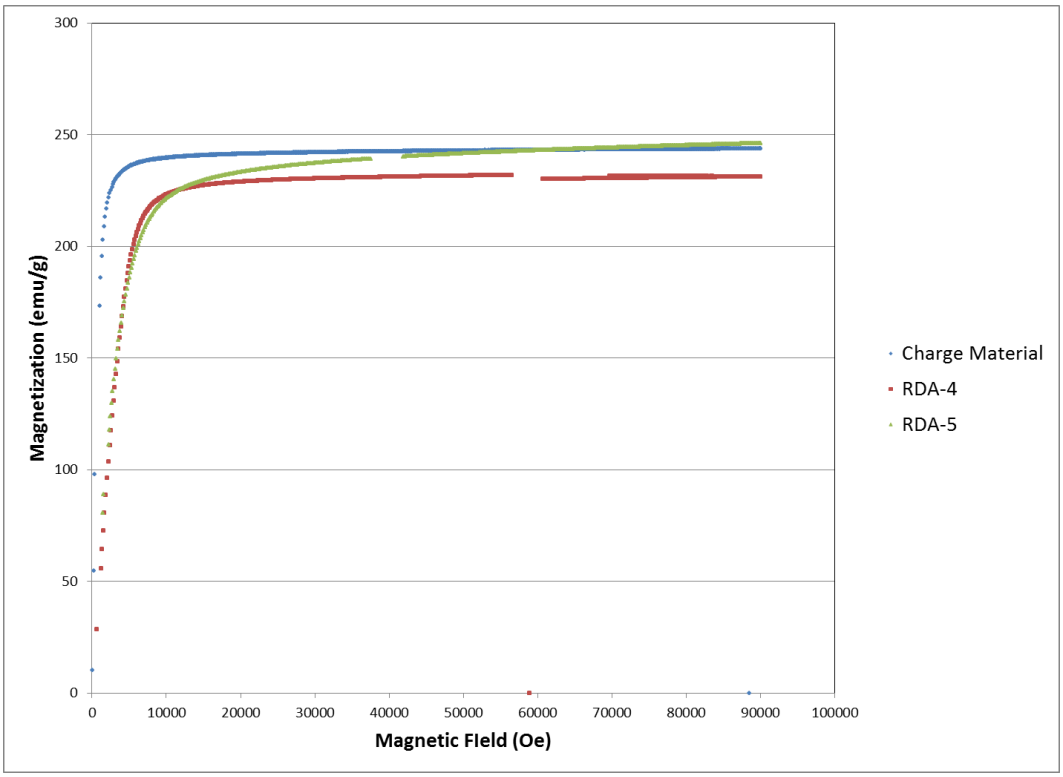

Figure 42: Gadolinium-Yttrium magnetic properties at 10K

The saturation values for these materials is similar for RDA-5 and its charge however the saturation values for RDA-4 is lower despite having lower contamination (Fig. 42). The LECO analysis does not seem to show the whole story for this type of alloy. There appears to be something going on in the magnetic properties that may be related to differences in charge chemistry. However for each powder the Curie temperature is desired but RDA-4 may lose some of the desired cooling effect due to its ~5% lower saturation magnetization.

CHAPTER 7

CONCLUSIONS AND FUTURE WORK

Conclusions

Gadolinium and gadolinium-yttrium powders are able to be produced using this rotating disk, rotating quench bath method of atomization. The powders can be made relatively spherical and with low enough contamination to lose only a small percent of the saturation magnetization compared to the charge material.

One of the most important variables to control in this process is the superheat applied. This has several consequences on the outcome of the atomization run. The lower the superheat applied the more likely the particles are to remain spherical. Superheat also appears to lower the oxygen level in the powders and raise the saturation magnetization of the resulting powder. The more spherical and lower the oxygen levels in the powders will create a better packing and more efficient refrigerator.

In order to improve this process the oil bath should be removed and a much larger inert chamber should be employed. This would solve several of the problems with this method of atomization. The drawback to this is that the atomizer itself would grow in size very substantially as the chamber would have to be very large to accommodate the solidification of the powders before they are able to contact the outer wall of the chamber. Further, any passivation benefits from the oil will not be achieved without the oil bath so passivation should be studied if this is to take place.

In order to increase the efficiency of the atomization process a better empirical predictive equation should be made to handle binary alloys that have a large “mushy” zone. The equation put forth by Champagne and Angers worked very well at predicting the particle

sizes when the charge used was pure Gadolinium but was ineffective at predicting parameters needed for the binary GdY alloy meaning several runs were performed that did not yield much usable particles. This would allow less preliminary runs to be made before finding the most ideal parameters for each particular alloy that need to be made.

Future Work

Another run of the gadolinium yttrium alloy should be completed to determine the most appropriate run parameters for this type of alloy. This run should include a redesign of the disk in order to prevent the disk deformation upon the shedding of the skull. This includes supporting the edge of the disk with the ceramic underneath as well as making the edges have a lower profile, while retaining their height above the center points of the disk. The full alloy chemistry should be determined to understand its effect on the magnetic properties of the materials.

Further alloy runs that are gadolinium based with heavy lanthanide alloying additions should be made to create a progression of alloys with lower and lower Curie temperatures. In order to liquefy Hydrogen the refrigerator will need to operate efficiently at lower temperatures than these alloys are capable of.

Another improvement that can be made is to pressurize the crucible in addition to the stopper rod. This would allow a more consistent liquid flow from the crucible to impinge on the disk. Also, the melt flow rate could be made more consistent by applying increased pressure in the crucible as the run goes evening out the flow rate.

X-ray diffraction measurements should be made on the powders compared to the charge materials in order to determine if there is a shift in the lattice parameter that occurs

due to interstitial contamination of the powders. It is also possible that the high temperature phases in gadolinium or the alloy could be present in the powder, but not in the bulk due to the large difference in their quench rates.

REFERENCES

[1]R. Drnevich, “Hydrogen delivery-liquefaction and compression. Praxair, strategic initiatives for hydrogen delivery workshop”-May 7, 2003

[2] Gschneidner, Mudryk, Pecharsky, Taken with permission

[3] K. A. Gschneidner Jr, V K Pecharsky, and A O Tsokol. Recent developments in magnetocaloric materials. Rep. Prog. Phys. , 68:1479– 1539, 2005.

[4]L.F. Aprigliano, G Green, J. Chafe, L. O’Connor, F. Biancello, and S. Ridder, “Development of neodymium and Er_3Ni regenerator materials,” Adv. In Cryog. Eng. 1992 1003-1009

[5]I.E. Anderson, M.G. Osborne, H. Takeya, and K.A. Gschneidner Jr., “Gas atomized Er_3Ni powder for cryocooler applications,” in Proceedings of the Seventh International Cryocooler Conference, Santa Fe, NM, Nov. 17-19, 1992, Doc #PL-CP-93-1003, pp. 1120-1132

[6] Nielsen K.K., “Magnetocaloric refrigeration concepts: current state of the art” TMS 2014, Annual Meeting & Exhibition, Supplemental Proceedings, 143rd, San Diego, CA, United States, Feb. 16-20, 2014 Nielsen, K yr:2014 pg:777 -784

[7] S. Krasae-in, J.H. Stang, P. Neksa, “Development of large-scale hydrogen liquefaction processes from 1898 to 2009” International Journal of Hydrogen Energy May 2010, pp. 4524-4533

[8]R.M German, In Powder Metallurgy Science, Metal Powder Industries Federation, Princeton, 1984, pp.81-86

[9]A. Lawley, “An overview of powder atomization processes and fundamentals,” Int. J. of Powd. Met. & Powd. Tech. 1977, 13, 169-188

[10]A. Lawley, “Atomization of specialty alloy powders, “J. of Metals 1981, 33, 13-18

[11]B. Champagne and R. Angers, “REP atomization mechanisms,” Powder Met. Int. 1984, 125-128

[12]H. Peng, N. Wang, D. Wang, X. Ling, “Experimental Study on the Critical Characteristics of Liquid Atomization by a Spinning Disc,” Ind. Eng. Chem. Res. 2016,6175-6185

[13]B. Champagne and R. Angers, “Size distributions of powders atomized by the rotating electrode process,” in Modern Developments in Powder Metallurgy, Proceedings of the 1980 International Powder Metallurgy Conference, 83-104

[14]M. Osborne, “Centrifugal atomization of Lanthanide Materials for Cryogenic Coolers.” MS thesis, Iowa State University, 1993.

[15] C. Labrecque, R. Angers, R. Tremblay & D. Dubé (1997) Inverted Disk Centrifugal Atomization of AZ91 Magnesium Alloy, Canadian Metallurgical Quarterly, 36:3, 169-175, DOI: 10.1179/cmq.1997.36.3.169

[16]R. Anderson, “Powder Metallurgy at Pratt & Whitney,” Int. J. of Powd. Met. 1990, 171-178

[17]K.S. Funke, “Development of a centrifugal atomization process for the production of large spherical metal powders,” MS Thesis, Iowa State University, 1991.

[18]Sungkhaphaitoon, Likhidkan, Kitjaidiaw, Wisutmethangoon, Plookphol, “Effect of Atomizer Disc Geometry on Zinc Metal Powder Production by Centrifugal Atomization,” Applied Mechanics and Materials 2013

[19]R. Angers, R. Tremblay, L. Desrosiers, D. Dube, “Rotating disk coatings for centrifugal atomization of aluminum and magnesium alloys,” Canadian Metallurgical Quarterly 1996, pp.291-297

[20]J .Barclay, private e-mail, September 2016

[21]O.S. Nichiporenko and Y.I. Naida: Sov. Powd. Metall. And Met. Ceramics, no. 10, pp.753-755

[22] Ishikawa, T., Okada, J.T., Paradis, PF. et al. Int J Thermophys (2010) 31: 388.

[23] A.K. Srivastava, "On cooling rates, interface velocities and particle sizes in spray atomization," Journal of Materials Science Letters 2000

[24] Gschniedner K.A. Jr., F.W. Calderwood, ASM phase Diagram Database, *accessed 10/2016*, published 1990

[25] B.J. Keene, "Review of data for the surface tension of pure metals," The Institute of Materials and ASM International. 1993

[26] Jiles D. Introduction to Magnetism and Magnetic Materials 1998. Pp. 68-69

[27] Riedmenn, Anderson, "Production of fine Ca powders by Centrifugal atomization with rotating quench bath"

[28] J.F. Elliot, S. Legvold, F. H. Spedding, "Some magnetic properties of gadolinium metal," Physical Review 1953

[29] "Claude Cycle" *http://platform.sysmoltd.com/ThermoFluids/LiquefactionCycles* Accessed 11-11-16

[30] Zimm C, Jastrab A, Sternberg A, Pecharsky V and Geschneidner K Jr 1998 *Adv. Cryog. Eng.* **43** 1759-66

[31] Costa G., Kaiser E., "Structural and thermal properties in Gd-Y magnetic alloys," Thermochimica Acta 1993 107-115

[32] Kurt J. Lesker Company, "KJLC 704 Specifications table" http://www.lesker.com/newweb/fluids/diffpumpoils_silicone_kjlc.cfm?pgid=704